ORTA DOĞU TEKNİK ÜNİVERSİTESİ
FEN BİLİMLERİ ENSTİTÜSÜ MÜDÜRLÜĞÜ

TEZ ŞABLONU ONAY FORMU
THESIS TEMPLATE CONFIRMATION FORM

1. Şablonda verilen yerleşim ve boşluklar değiştirilmemelidir.
2. **Jüri tarihi** Başlık Sayfası, İmza Sayfası, Abstract ve Öz'de ilgili yerlere yazılmalıdır.
3. İmza sayfasında jüri üyelerinin unvanları doğru olarak yazılmalıdır. Tüm imzalar **mavi pilot kalemle** atılmalıdır.
4. **Disiplinlerarası** programlarda görevlendirilen öğretim üyeleri için jüri üyeleri kısmında tam zamanlı olarak çalıştıkları anabilim dalı başkanlığının ismi yazılmalıdır. Örneğin: bir öğretim üyesi Biyoteknoloji programında görev yapıyor ve biyoloji bölümünde tam zamanlı çalışıyorsa, İmza sayfasına biyoloji bölümü yazılmalıdır. İstisnai olarak, disiplinler arası program başkanı ve tez danışmanı için disiplinlerarası program adı yazılmalıdır.
5. Tezin **son sayfasının sayfa** numarası Abstract ve Öz'de ilgili yerlere yazılmalıdır.
6. Bütün chapterlar, referanslar, ekler ve CV sağ sayfada başlamalıdır. Bunun için **kesmeler** kullanılmıştır. **Kesmelerin kayması** fazladan boş sayfaların oluşmasına sebep olabilir. Bu gibi durumlarda paragraf (¶) işaretine tıklayarak kesmeleri görünür hale getirin ve yerlerini **kontrol edin**.
7. Figürler ve tablolar kenar boşluklarına taşmamalıdır.
8. Şablonda yorum olarak eklenen uyarılar dikkatle okunmalı ve uygulanmalıdır.
9. Tez yazdırılmadan önce PDF olarak kaydedilmelidir. Şablonda yorum olarak eklenen uyarılar PDF dokümanında yer almamalıdır.
10. Tez taslaklarının kontrol işlemleri tamamlandığında, bu durum öğrencilere METU uzantılı öğrenci e-posta adresleri aracılığıyla duyurulacaktır.
11. Tez yazım süreci ile ilgili herhangi bir sıkıntı yaşarsanız, Sıkça Sorulan Sorular (SSS) sayfamızı ziyaret ederek yaşadığınız sıkıntıyla ilgili bir çözüm bulabilirsiniz.

1. Do not change the spacing and placement in the template.
2. Write **defense date** to the related places given on Title page, Approval page, Abstract and Öz.
3. Write the titles of the examining committee members correctly on Approval Page. **Blue ink** must be used for all signatures.
4. For faculty members working in **interdisciplinary programs**, the name of the department that they work full-time should be written on the Approval page. For example, if a faculty member staffs in the biotechnology program and works full-time in the biology department, the department of biology should be written on the approval page. Exceptionally, for the interdisciplinary program chair and your thesis supervisor, the interdisciplinary program name should be written.
5. Write **the page number of the last page** in the related places given on Abstract and Öz pages.
6. All chapters, references, appendices and CV must be started on the right page. **Section Breaks** were used for this. **Change in the placement** of section breaks can result in extra blank pages. In such cases, make the section breaks visible by clicking paragraph (¶) mark and **check their position.**
7. All figures and tables must be given inside the page. Nothing must appear in the margins.
8. All the warnings given on the comments section through the thesis template must be read and applied.
9. Save your thesis as pdf and Disable all the comments before taking the printout.
10. This will be announced to the students via their METU students e-mail addresses when the control of the thesis drafts has been completed.
11. If you have any problems with the thesis writing process, you may visit our Frequently Asked Questions (FAQ) page and find a solution to your problem.

☒ **Yukarıda bulunan tüm maddeleri okudum, anladım ve kabul ediyorum. / I have read, understand and accept all of the items above.**

Name :
Surname :
E-Mail :
Date :
Signature : _____

COMPARATIVE SEISMIC PERFORMANCE ASSESSMENT OF BASE ISOLATED BUILDINGS WITH FRICTION PENDULUM BEARINGS DUE TO UPLIFT ASSOCIATED IMPACT EFFECTS

A THESIS SUBMITTED TO
THE GRADUATE SCHOOL OF NATURAL AND APPLIED SCIENCES
OF
MIDDLE EAST TECHNICAL UNIVERSITY

BY

GÖKSEL ÇALLI

IN PARTIAL FULFILLMENT OF THE REQUIREMENTS
FOR
THE DEGREE OF MASTER OF SCIENCE
IN
ENGINEERING SCIENCES

APRIL 2024

Approval of the thesis:

COMPARATIVE SEISMIC PERFORMANCE ASSESSMENT OF BASE ISOLATED BUILDINGS WITH FRICTION PENDULUM BEARINGS DUE TO UPLIFT ASSOCIATED IMPACT EFFECTS

submitted by **GÖKSEL ÇALLI** in partial fulfillment of the requirements for the degree of **Master of Science** i**n Engineering Sciences, Middle East Technical University** by,

Prof. Dr. Naci Emre Altun
Dean, Graduate School of **Natural and Applied Sciences** _____

Prof. Dr. Murat Dicleli
Head of the Department, **Engineering Sciences** _____

Assist. Prof. Dr. Murat Dicleli
Supervisor, **Engineering Sciences, METU** _____

Examining Committee Members:

Assist. Prof. Dr. Mustaf Tolga Yılmaz
Engineering Science, METU _____

Prof. Dr. Murat Dicleli
Engineering Science, METU _____

Prof. Dr. Ahmet Hakan Argeşo
Aerospace Engineering, Atılım University _____

Date: 26.04.2024

I hereby declare that all information in this document has been obtained and presented in accordance with academic rules and ethical conduct. I also declare that, as required by these rules and conduct, I have fully cited and referenced all material and results that are not original to this work.

Name Last name : Göksel Çallı

Signature :

ABSTRACT

COMPARATIVE SEISMIC PERFORMANCE ASSESSMENT OF BASE ISOLATED BUILDINGS WITH FRICTION PENDULUM BEARINGS DUE TO UPLIFT ASSOCIATED IMPACT EFFECTS

Çallı, Göksel
Master of Science, Engineering Sciences
Supervisor: Prof. Dr. Murat Dicleli

April 2024, 75 pages

This thesis investigates the impact of seismic isolation on enhancing building resilience in earthquake-prone areas, focusing specifically on the uplift effects of friction pendulum bearings. Friction pendulum bearings are critical in decoupling buildings from ground motions, thereby mitigating the transfer of seismic energies and reducing structural damage. Friction pendulum bearings are notable for their ability to absorb and dissipate earthquake forces through a pendulum-like sliding motion, returning the structure to its original position post-earthquake.

This research uses a 2D modeling approach on SAP 2000 to analyze 21 buildings with varying characteristics such as the number of stories, bays, curvature radius of the sliding surfaces of friction pendulum bearings, friction coefficients of friction pendulum bearings, peak ground accelerations, and soil classifications. The analysis extends to examining the effects of different column foundation connections and variations in structural components like shear walls and isolator level beams on the uplift behavior of the bearings. The aim is to enhance the operational integrity of

essential facilities such as hospitals and emergency centers, contributing to safer infrastructure development in seismic zones. This study not only furthers the understanding of seismic isolation components but also seeks to improve the seismic resilience of modern structures.

Keywords: Uplift and Impact Effect, Equivalent Linear Analysis, Time History Analysis, Seismic Base Isolation, Earthquake

ÖZ

KALKMA İLE İLİŞKİLİ DARBE ETKİSİ NEDENİYLE SÜRTÜNMELİ SARKAÇ MESNETLİ TABAN İZOLASYONLU BİNALARIN KARŞILAŞTIRMALI SİSMİK PERFORMANS DEĞERLENDİRMESİ

Çallı, Göksel
Yüksek Lisans, Mühendislik Bilimleri
Tez Yöneticisi: Prof. Dr. Murat Dicleli

Nisan 2024, 72 sayfa

Bu tez, depreme dayanıklı bölgelerde bina dayanıklılığını artırmak amacıyla sismik izolasyonun etkilerini incelemekte olup, özellikle sürtünmeli sarkaç mesnetlerin kaldırma etkilerine odaklanmaktadır. Sürtünmeli sarkaç mesnetler binaları yer hareketlerinden ayırarak sismik enerjilerin aktarımını azaltmakta ve yapısal hasarı minimize etmektedir. Sürtünmeli sarkaç mesnetler, bir sarkaç gibi kayan hareketlerle deprem kuvvetlerini emme ve dağıtma yetenekleriyle dikkat çekmektedir; bu sayede yapıyı deprem sonrası orijinal pozisyonuna geri döndürebilmektedir.

Bu araştırma, SAP 2000 üzerinde 2D modelleme yaklaşımı kullanarak, kat sayısı, kiriş aralıkları, sürtünmeli sarkaç mesnetlerin kayma yüzeylerinin eğrilik yarıçapı, sürtünmeli sarkaç mesnetlerin sürtünme katsayıları, zemin sınıflandırmaları ve en büyük yer ivmeleri gibi çeşitli özelliklere sahip 21 binayı analiz etmektedir. Analiz, farklı kolon temel bağlantılarının ve kesme duvarları ile izolatör temel kirişlerindeki yapısal değişikliklerin yatakların kaldırma davranışları üzerindeki etkilerini incelemektedir. Bu çalışmanın amacı, hastaneler ve acil durum merkezleri gibi hayati

tesislerin operasyonel bütünlüğünü artırarak, deprem bölgelerinde daha güvenli altyapı gelişimine katkıda bulunmaktır. Bu çalışma, sadece sismik izolasyon bileşenlerinin anlaşılmasını ilerletmekle kalmayıp, aynı zamanda modern yapıların sismik dayanıklılığını iyileştirmeyi hedeflemektedir.

Anahtar Kelimeler: Kalkma Ve Darbe Etkileri, Eşdeğer Doğrusal Analiz, Zaman Tanım Alanında Analiz, Sismik Taban İzolasyonu, Deprem

To my wife Özgür and my daughter Öykü.

ACKNOWLEDGMENTS

I wish to express my deepest gratitude to my supervisor Prof. Dr. Murat Dicleli for his guidance, advice, criticism, encouragements and during my thesis study.

Secondly, I am gratefully to Ender Başar who is my project director at ALARKO, for his support and companionship.

Finally, I would like to thank my wife Özgür Çallı, my daughter Öykü Çallı, my mother Süheyla Çallı and My Father Nurettin Çallı. This thesis is dedicated to them. Without their love and belief in me; I would never have accomplished this.

TABLE OF CONTENTS

LIST OF TABLES

TABLES

LIST OF FIGURES

FIGURES

CHAPTER 1

INTRODUCTION

1.1 Introduction

Seismic isolation has become an essential strategy in earthquake engineering, particularly in regions susceptible to seismic activities. This approach involves the construction of buildings and other structures with specialized isolation systems designed to absorb and dissipate earthquake energy. By mitigating the transfer of energy from the ground to the building, seismic isolation not only reduces structural shaking but also significantly enhances the building's resilience to earthquake-induced stresses.

Seismic isolators, typically installed at the base of a structure, come in various forms including base isolators, rubber bearings, and sliders. These devices allow the building to move independently from ground motions, effectively reducing the impact of the forces. Such innovative designs are crucial for maintaining the operational integrity of critical facilities like hospitals, emergency response centers, and bridges, even after significant seismic events. The widespread adoption of these technologies has fostered the development of safer and more resilient infrastructures, thereby safeguarding lives and minimizing economic losses in earthquake-prone areas.

Friction pendulum bearings are a popular choice for seismic isolation. These systems combine sliding mechanisms and pendulum dynamics to efficiently manage the energy released during an earthquake, th ereby minimizing structural damage. The

operation of friction pendulum bearings involves a pendulum-like motion, where sliding occurs along a concave surface. This mechanism enables the structure to sway horizontally during an earthquake, reducing the forces transmitted through the building. After the earthquake, the curved surface of the bearing guides the structure back to its original position, ensuring stability and alignment.

In this research, the uplift effect on friction pendulum bearings was evaluated. A selection of 21 buildings was made to examine the rocking effect on friction pendulum bearings. Key variable parameters included the number of stories and bays in the buildings, the curvature radius of the sliding surfaces on the friction pendulum bearings, the friction coefficient of these bearings, peak ground acceleration, and soil site classification. The buildings were modeled using SAP 2000, a structural analysis and design software, employing a 2D modeling approach to assess the impact of varying structural parameters on building performance. The structural analysis models were based on the master thesis "Effect of the Number of Stories and Aspect Ratio on the Seismic Performance of Base Isolated Buildings," supervised by Prof. Dr. Murat Dicleli and submitted by Oğuz Zerman. To evaluate the impact effect in 2D models with friction pendulum bearings, various column foundation connection types were developed: uplift allowed system (UAS), uplift restrained system (URS), and uplift allowed impact modeled system (UAIMS).

Additionally, the study explored how variations in shear wall and isolator level beam dimensions influence the uplift effect. This comprehensive analysis aims to refine our understanding of seismic isolation components and their functionality, enhancing the seismic resilience of structures.

1.2 Literature Review

This literature review synthesizes pivotal studies from 1963 through 2024, focusing on the seismic performance of base-isolated buildings using friction pendulum

bearings, with particular attention to the uplift and impact effects enhanced by column rocking and bearing rocking mechanisms. These studies collectively advance our understanding of how different isolation and structural dynamics strategies can be integrated to improve the seismic resilience of buildings.

The exploration of rocking mechanisms in seismic design began with George W. Housner's 1963 article, "The behavior of inverted pendulum structures during earthquakes." This seminal work introduced the concept of buildings behaving like inverted pendulums, significantly influencing subsequent developments in seismic isolation.In 1982, practical observations from "The response of veterans hospital building 41 in the San Fernando earthquake" provided real-world evidence of the effectiveness of early seismic isolation strategies, underscoring the importance of understanding building dynamics during earthquakes."Simplified Earthquake Analysis of Structures With Foundation Uplift" (1985) marked a significant advancement in the analytical approach to understanding how buildings interact with seismic forces, particularly focusing on the phenomena of uplift and its implications for building stability.The early 2000s brought a deeper integration of rocking mechanisms with seismic isolation strategies. "Earthquake response reduction of buildings by rocking structural systems" (2002) and "Seismic response reduction of steel frames with multi-spans by applying rocking structural system" (2006) discussed the benefits of using rocking systems to reduce seismic responses across different building configurations.More sophisticated applications were explored through "Modeling and seismic response of structures with concrete rocking columns and viscous dampers" (2010), which integrated damping systems with rocking columns for enhanced performance. This study was followed by detailed investigations into the dynamic interactions within rocking systems in "The interaction of elasticity and rocking in flexible structures allowed to uplift" (2012) and "Robust Modeling of the Rocking Problem" (2012).The mid-2010s and early 2020s saw significant innovations in controlled rocking systems and the introduction of negative stiffness properties. "Dynamic and equivalent static procedures for

capacity design of Controlled rocking steel braced frames" (2016) and "New rocking column with control of negative stiffness displacement range and its application to RC frames" (2020) offered new insights into the controlled application of rocking dynamics to enhance seismic isolation.Recent experimental studies like "Experimental study on seismic performance of RC frames with Energy-Dissipative Rocking Column system" (2019) and analytical advancements in "Displacement-based analysis and design of rocking structures" (2019) have provided crucial data and methodologies for refining the design and implementation of rocking systems in seismic engineering.Reflecting on long-term strategies, "A half-century of rocking isolation" (2014) and "The role of the rotational inertia on the seismic resistance of free-standing rocking columns and articulated frames" (2014) evaluated the historical development and theoretical contributions to rocking isolation technologies, underscoring their sustained relevance and effectiveness.

The reviewed literature from 1963 to 2024 demonstrates the significant evolution of seismic isolation techniques. These studies highlight the complex interplay of uplift and impact effects within these systems, offering valuable insights into designing more resilient structures capable of withstanding severe seismic events. The ongoing research and development in this area continue to push the boundaries of seismic engineering, ensuring that modern and future buildings can achieve the highest levels of safety and functionality during earthquakes.

Building on previous research, the objective of this study is to conduct a comparative seismic performance assessment for uplift and impact effects of friction pendulum bearings in base-isolated buildings. This analysis will focus on varying key parameters including the number of stories and bays in the buildings, the curvature radius of the sliding surfaces on the friction pendulum bearings, the friction coefficient of these bearings, peak ground acceleration, and soil site classification.

CHAPTER 2

PARAMETERS

2.1 Selected Parameters

To assess the rocking effects of friction pendulum bearings, a set of 21 buildings has been selected for detailed analysis. The dimensions of the selected buildings and floors, along with the properties of the friction pendulum bearings, are shown in Figures 2.1 and 2.2, respectively.

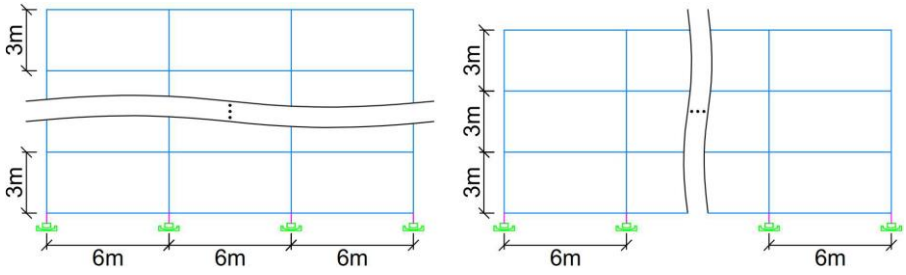

Figure 2.1. Selected Buildings Floors and Bays Dimensions

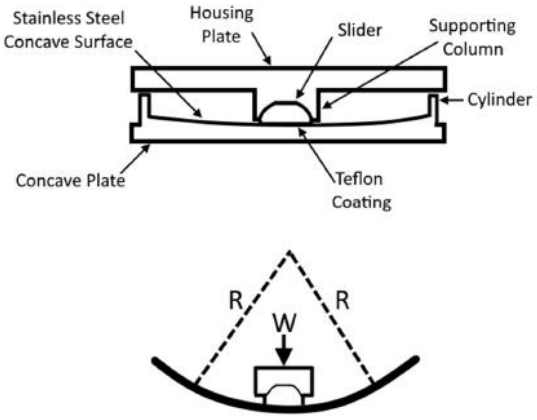

Figure 2.2. Selected Friction Pendulum Bearing Properties

The evaluation examines how variations in key structural and geological parameters affect the performance of these bearings during seismic events. These parameters include:

1. Building Story Number: Refers to the total number of floors within each building. This factor is crucial as the height of a building can influence its seismic response and the effectiveness of the friction pendulum bearings in mitigating rocking motions.

2. Building Bay Number: Indicates the number of openings or segments along the width of the building. This can affect the lateral stiffness and mass distribution, thereby influencing how a building rocks during an earthquake.

3. Sliding Surface Curvature Radius of Friction Pendulum Bearings: This parameter describes the curved surface over which the pendulum bearing slides during seismic activity. The radius of this curvature directly affects the trajectory and amplitude of the building's sway, impacting how energy is dissipated.

4. Friction Coefficient of Friction Pendulum Bearings: The friction coefficient determines the resistance between the sliding interfaces of the bearing. A higher friction coefficient generally results in greater resistance to sliding, which can affect the bearing's ability to reduce seismic forces.

5. Peak Ground Acceleration: This is a measure of the intensity of earthquake shaking at a site, expressed as a rate of acceleration. It is a critical parameter as it directly impacts the demand placed on the friction pendulum bearings during an earthquake.

6. Soil Site Classification: Different soil types can amplify or dampen seismic waves differently, affecting the movement experienced at the surface and thus the performance of seismic isolation systems like friction pendulum bearings.

A building featuring an 8-story, 5-bay structure has been chosen as the benchmark for analysis. This building incorporates a friction pendulum bearing system with a

sliding surface curvature radius of 5 meters and a friction coefficient of 5%. Additionally, it is subjected to a peak ground acceleration (PGA) of 0.8g and is situated on soil classified as Site Class C. The parameters selected for this analysis are detailed in Table 2.1.

Table 2.1 Selected Parameters for Analysis

	Friction Pendulum Bearings Properties		Building Properties			
Model Number	R(m)	μ	Story Number	Bay Number	PGA	Soil Site Classification
1	3	5%	8	5	0.8	C
2	5	5%	8	5	0.8	C
3	7	5%	8	5	0.8	C
4	5	3%	8	5	0.8	C
	5	5%	8	5	0.8	C
5	5	7%	8	5	0.8	C
6	5	5%	4	5	0.8	C
	5	5%	8	5	0.8	C
7	5	5%	12	5	0.8	C
8	5	5%	16	5	0.8	C
9	5	5%	8	3	0.8	C
	5	5%	8	5	0.8	C
10	5	5%	8	7	0.8	C
11	5	5%	8	5	0.4	C
	5	5%	8	5	0.8	C
12	5	5%	8	5	1.2	C
13	5	5%	8	5	1.6	C
14	5	5%	8	5	0.8	A/B
	5	5%	8	5	0.8	C
15	5	5%	8	5	0.8	D

Benchmark Model
Changing Properties

In addition to the previously selected parameters for analysis, those of a 12-story building, as detailed in Table 2.2, were also chosen to assess extreme cases.

Table 2.2 Extreme Cases Selected Parameters for Analysis

EXTREME CASES

	Friction Pendulum Bearings Properties		Building Properties			
MODEL NUMBER	R(m)	μ	Story Number	Bay Number	PGA	Soil Site Classification
16	5	3%	12	3	0.8	C
17	5	5%	12	3	0.8	C
18	5	7%	12	3	0.8	C
19	5	5%	12	3	0.4	C
	5	5%	12	3	0.8	C
20	5	5%	12	3	1.2	C
21	5	5%	12	3	1.6	C

Benchmark Model

Changing Properties

2.2 Response Spectum Function

Response spectrum functions are developed in compliance with the ASCE 7-10 standard for a specific location with coordinates 33.93147 N, 118.41442 W and Risk Category IV. The spectral accelerations are calculated for peak ground accelerations (PGA) of 0.2g, 0.4g, 0.6g, and 0.8g. The specified location and Risk Category IV are essential for determining the seismic parameters from the seismic hazard maps or through online seismic design tools such as the USGS Seismic Design Maps tool. Risk Category IV is chosen due to the critical nature of the facility being considered. Spectral Acceleration (S_a) is calculated using the formulas from ASCE 7-10. First, the mapped spectral accelerations (S_S and S_1) for short periods and 1s period respectively are determined. Next, the mapped spectral accelerations are adjusted for site effects using site coefficients (F_a and F_v). The formulas used are:

$$S_{MS} = F_a S_S \qquad (2.1)$$

$$S_{M1} = F_v S_1 \qquad (2.2)$$

These adjusted values account for the local site conditions. Then, the design spectral response accelerations (S_{DS} and S_{D1}) are calculated using the formulas:

$$S_{DS} = \frac{2}{3} S_{MS} \qquad (2.3)$$

$$S_{D1} = \frac{2}{3} S_{M1} \qquad (2.4)$$

Once the design spectral accelerations are calculated, the response spectrum functions can be constructed as outlined in ASCE 7-10 Section 11.4.5 for different periods (T) as follows:

- For $0 \leq T \leq T_0$

$$S_{(T)}=S_{DS}\times(0.4+0.6\frac{T}{T_0}) \quad (2.5)$$

- For $T_0 \leq T \leq T_S$ (2.6)

$$S_{(T)}=S_{DS}$$

- For $T_S \leq T \leq T_L$

$$S_{(T)}=S_{D1}/T \quad (2.7)$$

- For $T \geq T_L$

$$S_{(T)}=S_{D1}\times(T_L/T^2) \quad (2.8)$$

Here,

T_0 is defined as the period at the intersection of the initial linear rise and the constant plateau of the spectrum.

T_S is defined as the transition period, at which the spectral acceleration changes from being constant (flat) to inversely proportional to the period (descending slope).

T_L is the long-period transition period, often specified in ASCE 7-10 for different regions.

Response spectrum function, compliant with the ASCE7-10 standard depicted in Figure 2.3.

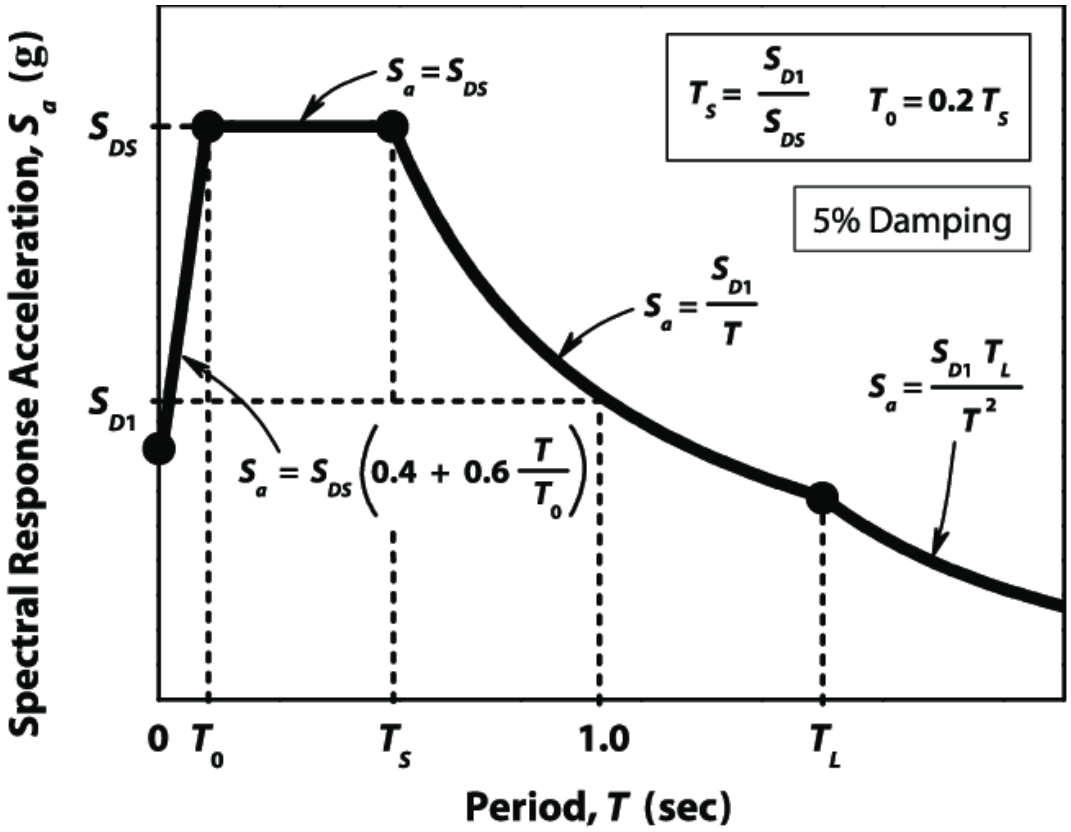

Figure 2.3. Response spectrum function, compliant with the ASCE7-10 standard.

The response spectrum functions for soil site classes A/B, C, and D, along with peak ground accelerations, are illustrated in Figures 2.4, 2.5, and 2.6, respectively.

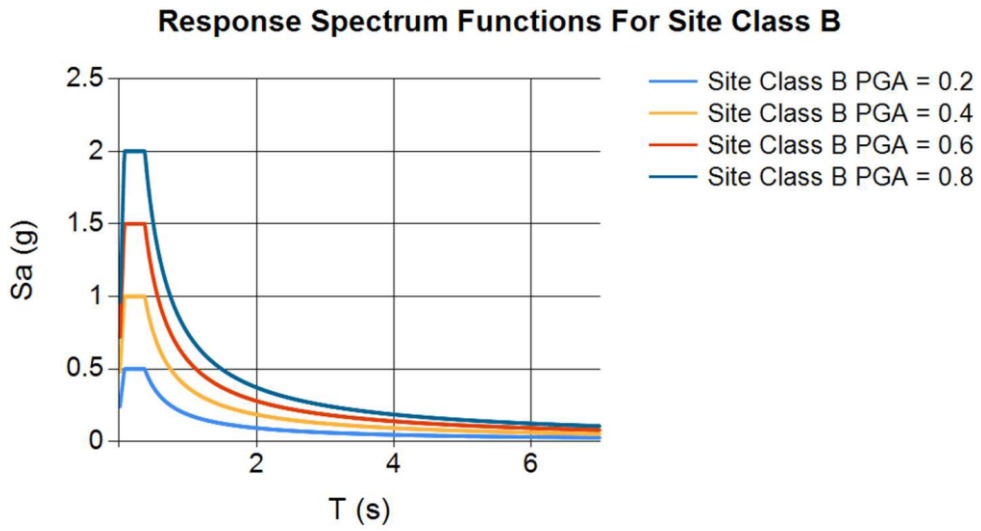

Figure 2.4. Response Spectrum Functions For Site Class A/B

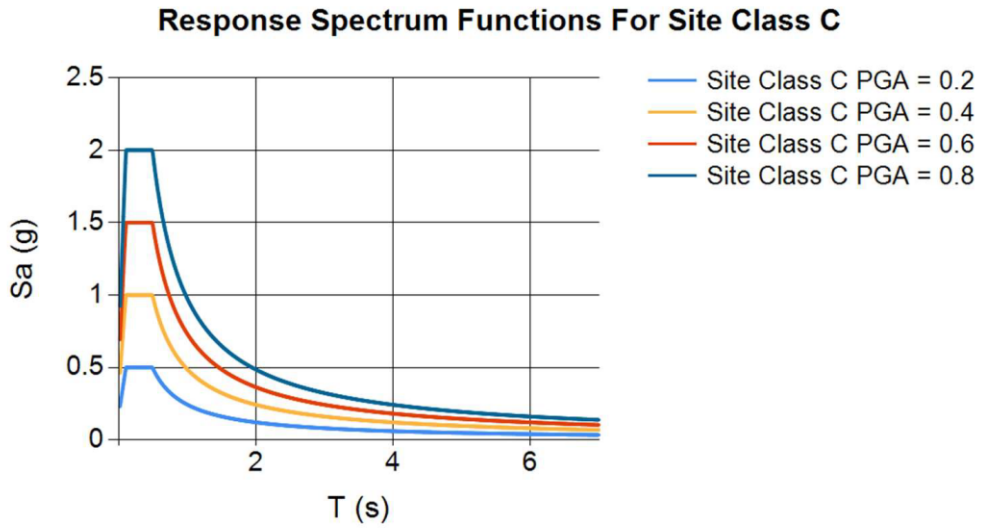

Figure 2.5. Response Spectrum Functions For Site Class C

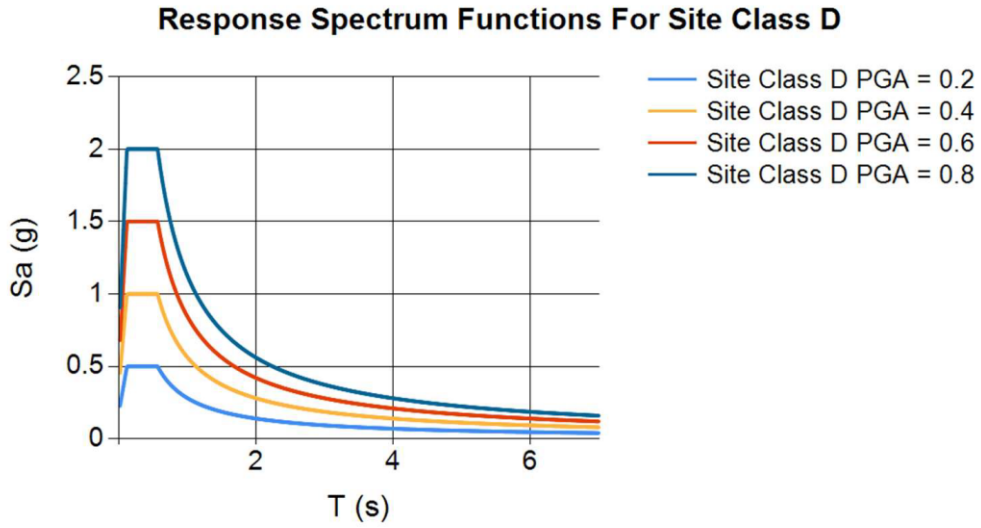

Figure 2.6. Response Spectrum Functions For Site Class D

CHAPTER 3

ROCKING AND IMPACT FORCE

3.1 Rigid Block Rocking and Coefficient of Restitution

Rigid block rocking, whose free body diagram is shown in Figure 3.1, is explained using a mathematical model by Housner [1]. Rocking block will oscillate about its centers of rotation O and O' when it undergoes rocking motion.

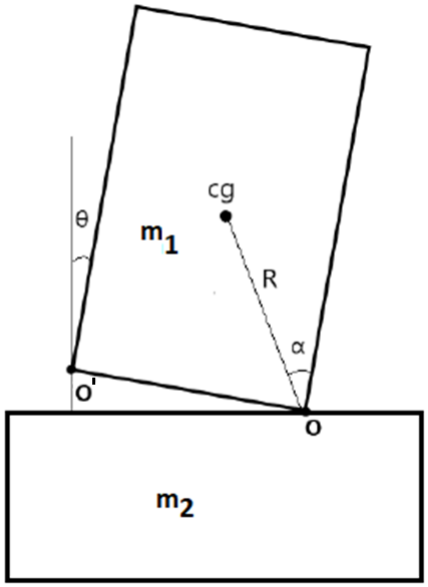

Figure 3.1. Free Body Diagram of the Rocking Block

Calculation of coefficient of restitution (CR) which is defined as the reduction in kinetic energy of the rocking body at impact is shown at Equation 3.1 [2].

$$CR = \left(1 - \frac{M_{eq}\mathrm{R}^2}{I_0}\,(1 - \cos 2\alpha)\right)^2 \tag{3.1}$$

M_{eq}: Equivalent mass of the two collapsing bodies.
R: Radial distance to the center of rotation.
I_0: Moment of inertia with respect to O or O' ($4/3M_{eq}R^2$)

3.2 Modelling Impact Effect of Pounding

The impact effect of colliding masses can be mathematically modeled, as depicted in Figure 3.2 [3]. This mathematical model encompasses a system of gap and link elements strategically positioned between the masses to accurately simulate the pounding phenomenon. The resulting impact force is a function of the damping coefficient (c) and stiffness coefficient (k), and it arises only when the gap between the colliding masses is closed.

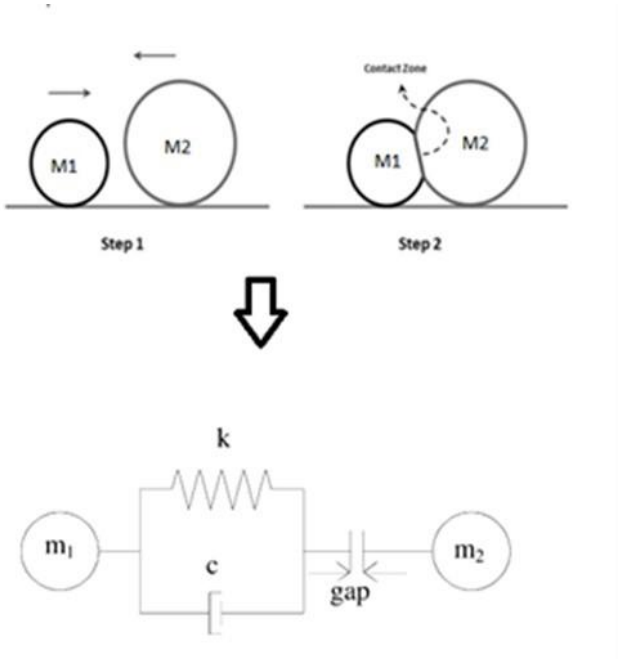

Figure 3.2. Mathematical Model For Impact Effect of Pounding

Mathematical model for impact effect of pounding can be represented by equivalent model as shown in Fig. 3.3.The Equation of motion for such a system will be:

Impact force

$$F_{imp}(t)=k_s\delta(t)+c_{imp}\dot{\delta}(t) \quad (3.2)$$

Equivalent Mass

$$M_{eq}=(m_1m_2)/(m_1+m_2) \quad (3.3)$$

Equivalent stiffness

$$k_s=(k_1 k_2)/(k_1+k_2) \quad (3.4)$$

Impact damping ratio

$$\xi_{imp}=\frac{-\ln(CR)}{\sqrt{\Pi^2+(ln(CR))^2}} \quad (3.5)$$

Impact damping coefficient

$$c_{imp}=2\xi_{imp}\sqrt{k_sM_{eq}} \quad (3.6)$$

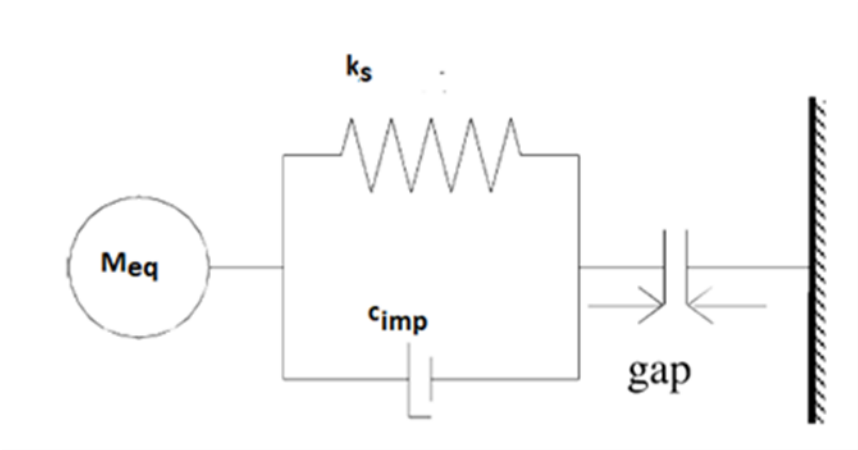

Figure 3.3. Equavalent Mathematical Model For Impact Effect of Pounding

To adapt the equvalent mathematical model for the impact effect of pounding to impact effect on a friction pendulum bearing, we need to redefine the parameters to fit this specific context. In this case, m_1 represents the total weight supported by the column, and m_2 represents the weight of the foundation. Similarly, k_1 is the axial rigidity of the column, and k_2 is the axial rigidity of the foundation. Using these parameters, we can calculate the impact force on the friction pendulum bearing by following the same methodology outlined from formula 3.2 to 3.6. First, the equivalent mass (M_{eq}) of the system is determined by formula 3.3 using the masses of the column and the foundation. Next, the equivalent stiffness (k_s) of the system is calculated by formula 3.4 based on the axial rigidities of the column and the foundation. It was assumed that a 1-meter-high raft foundation exists under all structures. Given that the distance between axes is 6 meters, each column was assumed to have a 3x3 isolated footing beneath it. The vertical stiffnesses of the foundations were then calculated based on this assumption. Impact damping coefficient (c_{imp}) is found by using formula 3.5 and 3.6. Finally, the impact force ($F_{\mathrm{imp}(t)}$) on the friction pendulum bearing is expressed by using formula 3.2.

CHAPTER 4

STRUCTURAL ANALYSIS MODEL

4.1 Building 2D Structural Analysis Model

4.1.1 Loads, Matrial Properties and Structural Elements Assigments

The buildings in this study were simulated using SAP 2000, a specialized software for structural analysis and design. A 2D modeling approach was adopted to enable a thorough evaluation of how various structural parameters influence building performance. The analytical models for the building structures draw from the master's thesis titled "Effect of the Number of Stories and Aspect Ratio on the Seismic Performance of Base Isolated Buildings," which was overseen by Prof. Dr. Murat Dicleli and authored by Oğuz Zerman. To calculate dead and live loads, ASCE/SEI 7-16 (2017) standards were followed, with the specific consideration that the structures are hospitals. The materials' self-weight, with concrete being 23.6 kN/m^2, was factored into the calculations. Visual representations of the benchmark model for the study can be found in Figures 4.1.

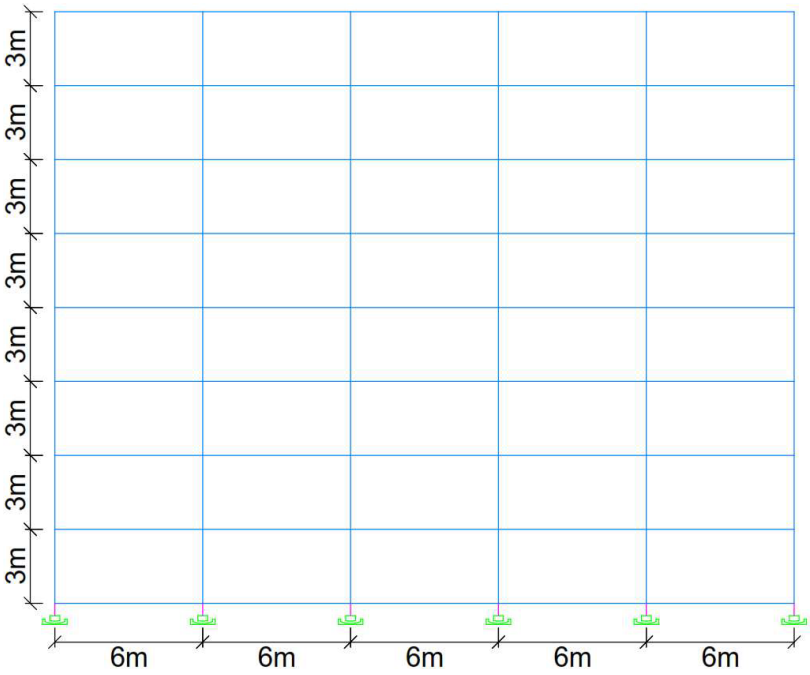

Figure 4.1.Benchmark Building 2D Model

The slab thicknesses have been set at 30 cm for the isolation level and 15 cm for the remaining stories. Dimensions of the column and beam section assignments can be found in Table 4.1.

Table 4.1 Dimensions of Column and Beam Members Assigned To the 2D Model

Story Number	Column Dimensions (cm)				Beam Dimensions (cm)			
	4 story	8 story	12 story	16 story	4 story	8 story	12 story	16 story
0	-	-	-	-	100x100	100x100	100x100	100x100
1	60x60	75x75	90x90	100x100	40x60	40x70	40x70	40x80
2	60x60	75x75	90x90	100x100	40x60	40x70	40x70	40x80
3	60x60	75x75	90x90	100x100	40x60	40x70	40x70	40x80
4	60x60	75x75	90x90	100x100	40x60	40x70	40x70	40x80
5	-	60x60	75x75	90x90	-	40x60	40x70	40x70
6	-	60x60	75x75	90x90	-	40x60	40x70	40x70
7	-	60x60	75x75	90x90	-	40x60	40x70	40x70
8	-	60x60	75x75	90x90	-	40x60	40x70	40x70
9	-	-	60x60	75x75	-	-	40x60	40x70
10	-	-	60x60	75x75	-	-	40x60	40x70
11	-	-	60x60	75x75	-	-	40x60	40x70
12	-	-	60x60	75x75	-	-	40x60	40x70
13	-	-	-	60x60	-	-	-	40x60
14	-	-	-	60x60	-	-	-	40x60
15	-	-	-	60x60	-	-	-	40x60
16	-	-	-	60x60	-	-	-	*40x60*

4.1.2 2D Models Friction Pendulum Bearing Assignment

The hysteresis loop for the friction pendulum bearing is depicted in Figure 4.2. The equation of motion for this system is as follows:

Initial stiffness

$$k_i = 100\frac{W}{R} \tag{4.1}$$

W: Weight on the seismic isolator
R: Sliding surface curvature radius

Characteristic strength

$$F_{yi} = \mu W \tag{4.2}$$

μ: Friction coefficient

Post-elastic stiffness

$$k_p = \frac{W}{R} \tag{4.3}$$

Equivalent stiffness

$$k_e = \frac{F_d}{D_d} = \frac{F_{yi}}{D_d} + k_p \tag{4.4}$$

D_d: Design displacement

Yield displacement

$$D_y = \frac{F_{yi}}{k_i - k_p} \tag{4.5}$$

Yield Force

$$F_y = D_y k_i \tag{4.6}$$

Design force

$$F_d = D_d k_e \tag{4.7}$$

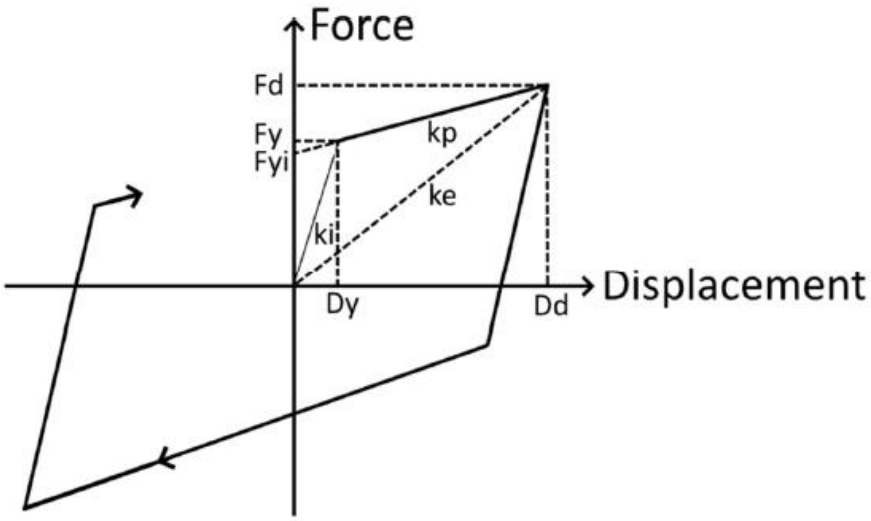

Figure 4.2.Hysteresis Loop of Friction Pendulum Bearing

Friction pendulum bearing hysteresis loop parameters which are assigned to 2D models are shown Table 4.2.

Table 4.2 2D Models Friction Pendulum Bearing Parameters

	Corner Columns Friction Pendulum Bearing Hysteresis Loop Parameters						Middle Columns Friction Pendulum Bearing Hysteresis Loop Parameters					
MODEL NUMBER	W(kN)	k_i (kN/m)	F_{yi} (kN)	k_p (kN/m)	D_Y (cm)	F_y (kN)	W(kN)	k_i (kN/m)	F_{yi} (kN)	k_p (kN/m)	D_Y (cm)	F_y (kN)
		100*W/R	μ*W	W/R	$F_{yi}/(k_i-k_p)$	D_y*k_i		100*W/R	μ*W	W/R	$F_{yi}/(k_i-k_p)$	D_y*k_i
1	2228,4	74280,3	111,4	742,8	0,152	112,5	3651,8	121725,2	182,6	1217,3	0,152	184,4
2	2228,4	44568,2	111,4	445,7	0,253	112,5	3651,8	73035,1	182,6	730,4	0,253	184,4
3	2228,4	31834,4	111,4	318,3	0,354	112,5	3651,8	52167,9	182,6	521,7	0,354	184,4
4	2228,4	44568,2	66,9	445,7	0,152	67,5	3651,8	73035,1	109,6	730,4	0,152	110,7
5	2228,4	44568,2	156,0	445,7	0,354	157,6	3651,8	73035,1	255,6	730,4	0,354	258,2
6	1201,0	24019,1	60,0	240,2	0,253	60,7	2089,3	41787,0	104,5	417,9	0,253	105,5
7	3391,2	67823,7	169,6	678,2	0,253	171,3	5240,4	104808,3	262,0	1048,1	0,253	264,7
8	4729,0	94579,1	236,4	945,8	0,253	238,8	6903,5	138070,6	345,2	1380,7	0,253	348,7
9	2225,9	44518,4	111,3	445,2	0,253	112,4	3604,8	72095,3	180,2	721,0	0,253	182,1
10	2225,6	44511,3	111,3	445,1	0,253	112,4	3662,2	73243,9	183,1	732,4	0,253	185,0
11	2228,4	44568,2	111,4	445,7	0,253	112,5	3651,8	73035,1	182,6	730,4	0,253	184,4
12	2228,4	44568,2	111,4	445,7	0,253	112,5	3651,8	73035,1	182,6	730,4	0,253	184,4
13	2228,4	44568,2	111,4	445,7	0,253	112,5	3651,8	73035,1	182,6	730,4	0,253	184,4
14	2228,4	44568,2	111,4	445,7	0,253	112,5	3651,8	73035,1	182,6	730,4	0,253	184,4
15	2228,4	44568,2	111,4	445,7	0,253	112,5	3651,8	73035,1	182,6	730,4	0,253	184,4
16	3390,0	67799,3	101,7	678,0	0,152	102,7	5122,1	102441,8	153,7	1024,4	0,2	155,2
17	3390,0	67799,3	169,5	678,0	0,253	171,2	5122,1	102441,8	256,1	1024,4	0,3	258,7
18	3390,0	67799,3	237,3	678,0	0,354	239,7	5122,1	102441,8	358,5	1024,4	0,4	362,2
19	3390,0	67799,3	169,5	678,0	0,253	171,2	5122,1	102441,8	256,1	1024,4	0,3	258,7
20	3390,0	67799,3	169,5	678,0	0,253	171,2	5122,1	102441,8	256,1	1024,4	0,3	258,7
21	3390,0	67799,3	169,5	678,0	0,253	171,2	5122,1	102441,8	256,1	1024,4	0,3	258,7

To evaluate the impact effects on 2D models equipped with friction pendulum bearings, several types of column foundation connections have been developed. These include the UAS, URS, and UAIMS. Each system is designed to simulate different conditions of uplift and restraint during seismic events, providing a detailed understanding of how these variables affect the overall seismic response of structures with friction pendulum bearings.

4.1.2.1 Uplift Allowed System (UAS)

In UAS; uplift effect is illuistrated for friction pendulum bearings as shown in the Figure 4.3.

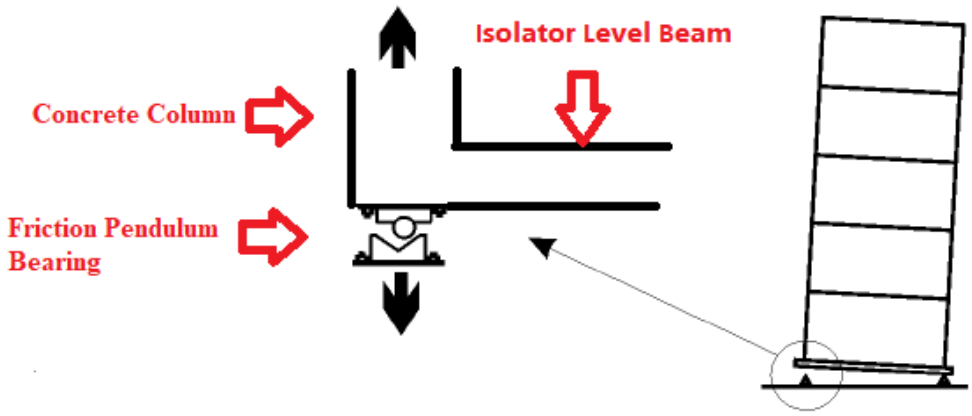

Figure 4.3. Uplift of Friction Pendulum Bearings

Rigid end zones are taken into consideration while generating the numerical model of the buildings as shown in the Figure 4.4.

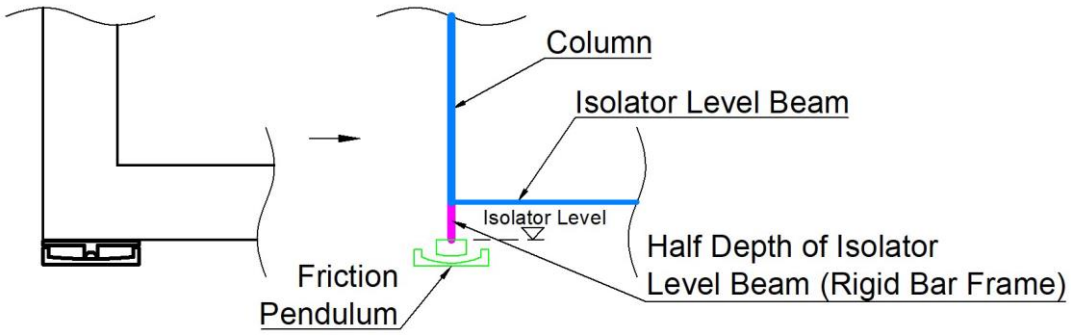

Figure 4.4. Numerical Model of UAS

Friction pendulum bearings are assigned as friction isolator links/supports in SAP 2000 models and cannot carry axial tension. Examples of the vertical and horizontal properties of these bearings assigned in SAP 2000 for UAS are displayed in Figures 4.5 and 4.6, respectively.

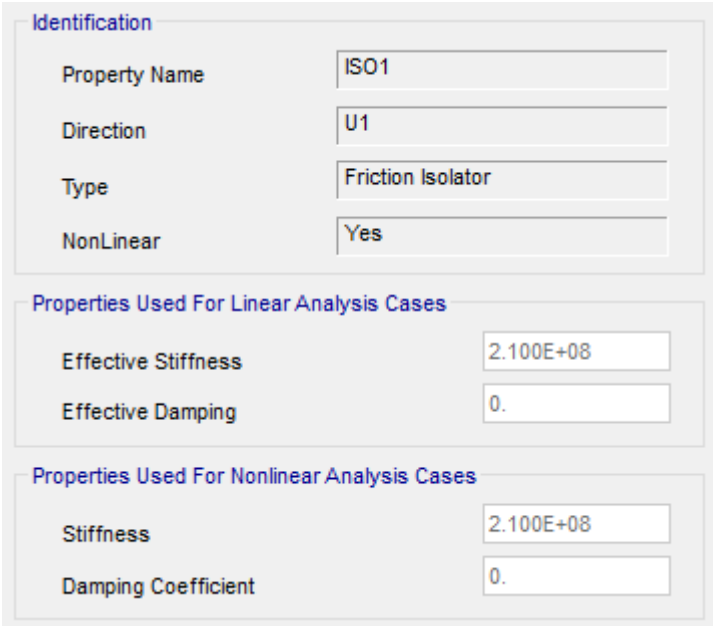

Figure 4.5. An Example Of Vertical Direction Properties Of Friction Pendulum Bearings Assigned In Sap 2000 For UAS (SI units kN,m)

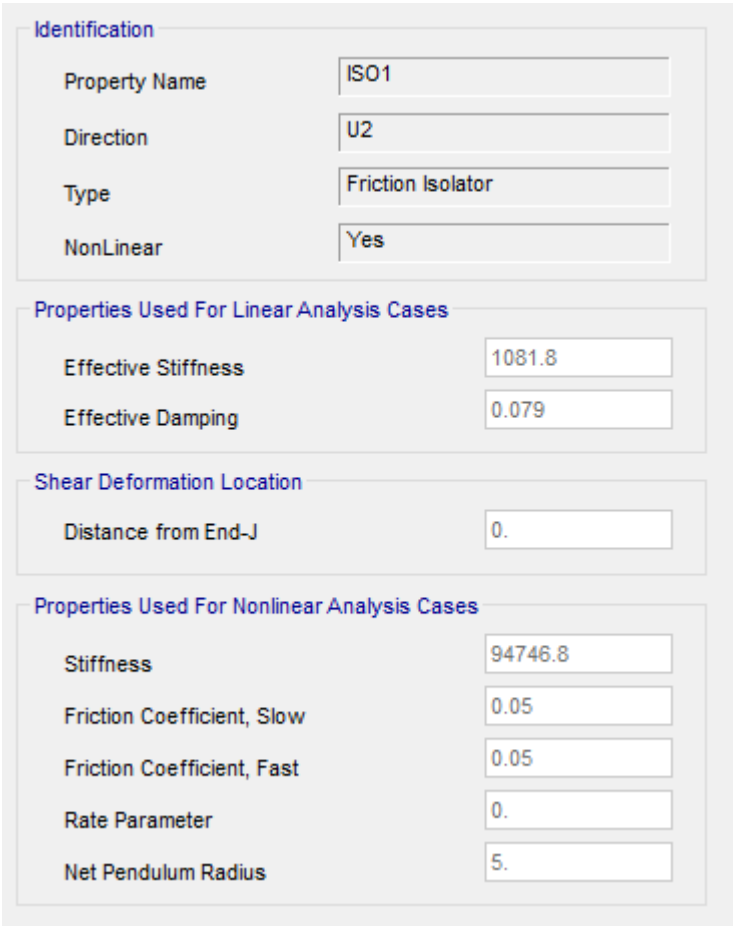

Figure 4.6. An Example Of Horizontal Direction Properties Of Friction Pendulum Bearings Assigned In Sap 2000 For UAS (SI units kN,m)

4.1.2.2 Uplift Restrained System (URS)

URS Sap 2000 models are adapted from uplift-allowed systems by modifying the friction isolator link/support type to a tension/compression friction isolator. In these systems, friction pendulum bearings are not limited to compression-only elements in the axial direction. Tensile forces that counteract the uplift of friction pendulum bearings have also been identified.

Examples illustrating the vertical and horizontal properties of friction pendulum bearings, as assigned in SAP 2000 for URS, are presented in Figures 4.7 and 4.8.

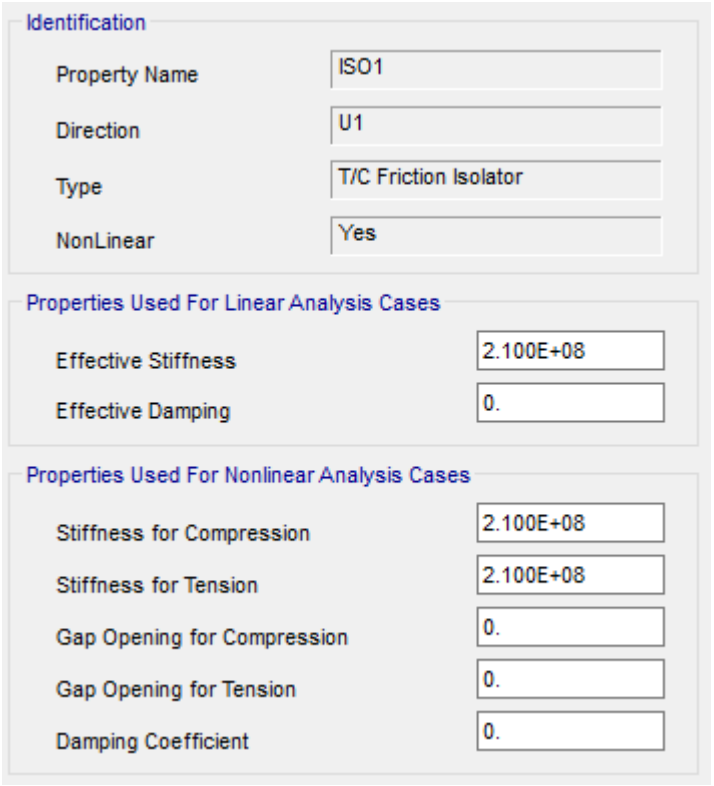

Figure 4.7. An Example Of Vertical Direction Properties Of Friction Pendulum Bearings Assigned In Sap 2000 For URS (SI units kN,m)

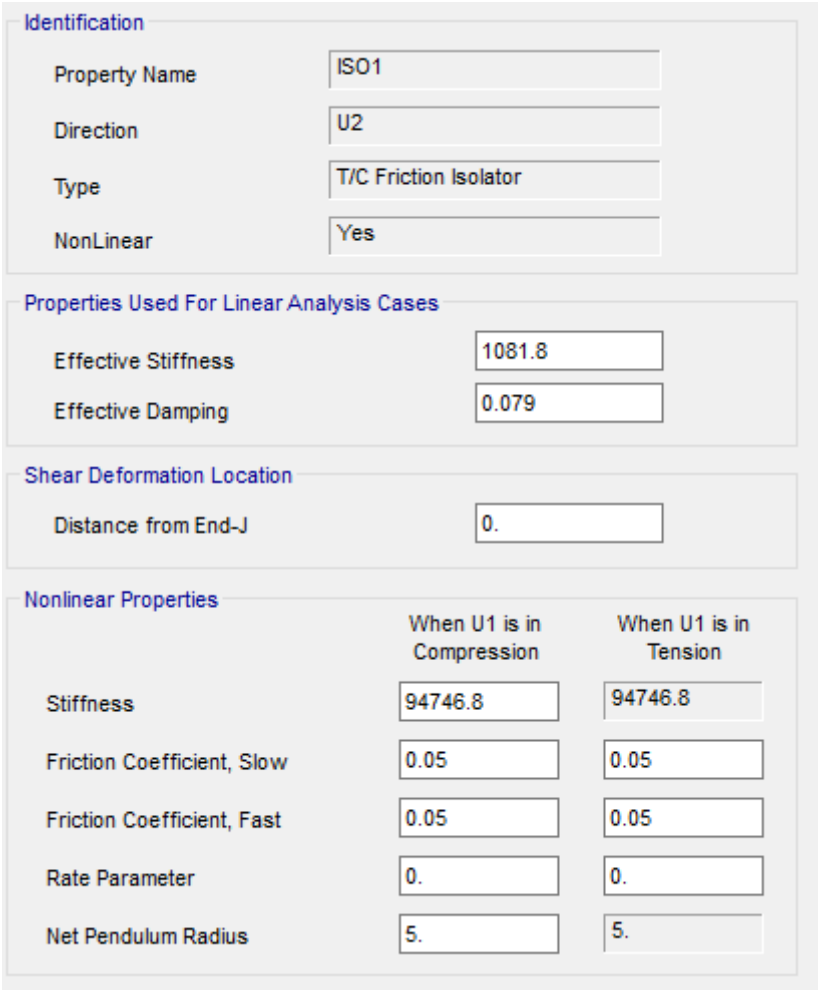

Figure 4.8. An Example Of Horizontal Direction Properties Of Friction Pendulum Bearings Assigned In Sap 2000 For URS (SI units kN,m).

4.1.2.3 Uplift Allowed Impact Modelled System (UAIMS)

The UAIMS SAP 2000 models are developed from UAS models with the additional specification of a damping coefficient, c_{imp}, to account for the impact force on friction pendulum bearings. The formula for calculating the impact force is detailed in Chapter 3.

$$F_{imp}(t)=k_s\delta(t)+c_{imp}\dot{\delta}(t) \quad (3.2)$$

Since there will not be vertical displacement at connection point of column to foundation; Impact force can be modelled, just as damping force, with a damping coefficient.

$$F_{imp}(t)=c_{imp}\dot{\delta}(t) \quad (4.1)$$

Damping due to impact force occurs only when the isolator is in compression, similar to a combination of a gap link element and a damper link element. An example of the damping coefficient properties that induce impact force in the vertical direction of friction pendulum bearings, as assigned in SAP 2000 for UAIMS, is illustrated in Figure 4.9.

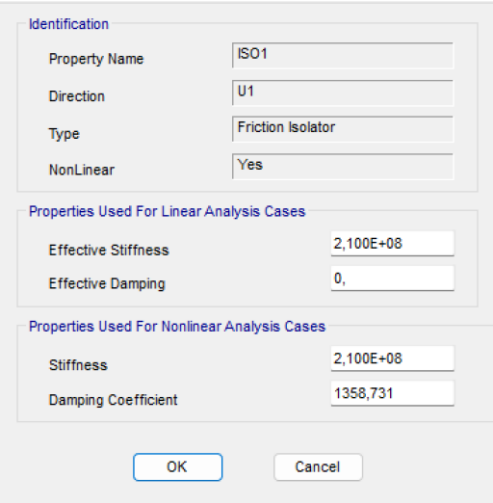

Figure 4.9. An Example Of Vertical Direction Properties Of Friction Pendulum Bearings Assigned In Sap 2000 For UAIMS (SI units kN,m)

CHAPTER 5

EQUIVALENT LINEAR ANALYSIS

An Equivalent Linear System for base isolated buildings is a simplified analytical approach that models the complex, nonlinear behavior of seismic isolation systems using linear properties. This method assumes that the isolation system can be represented by an effective stiffness and effective damping, which approximate its behavior under seismic loading. The effective stiffness is derived from the force-displacement relationship at the design displacement, while the effective damping reflects the energy dissipation characteristics of the isolation system, represented as an equivalent viscous damping ratio. By using these linearized properties, the Equivalent Linear System simplifies the analysis, making it more practical for preliminary design and assessment while still capturing the essential dynamic behavior of base isolated structures under seismic events.To properly adjust the ground motions mentioned in Chapter 6, it's crucial to ascertain the structure's effective period (Te) and the damping reduction factor (B). Dicleli & Buddaram [4] offer a comprehensive description of the iterative method used for the equivalent linear analysis of seismically isolated structures, as described below:

Step 1: Assume a design displacement (D_d) for the isolator.

Step 2: Calculate the effective stiffness (k_e) of the isolator from Eq. (4.4).

Step 3: Calculate the seismic-isolated structure effective stiffness by summing all the friction pendulum bearing effective stiffness (k_e) and seismic-isolated structure mass.

Step 4: Calculate the viscous damping ratio of structure (ζ_e).

$$\zeta_e = \frac{4\times\sum F_{yi}\times(D_d - D_Y)}{2\times\pi\times\sum k_e\times {D_Y}^2} \quad (5.1)$$

Step 5: Calculate the seismic equivalent effective period of structure.

$$T_e = 2\pi\sqrt{\frac{\sum\frac{w}{g}}{\sum k_e}} \quad (5.2)$$

Step 6: Calculate the seismic damping reduction factor (B).

$$\mathrm{B} = \left(\frac{\zeta_e}{0.05}\right)^3 \quad (5.3)$$

Step 7 : Obtain the spectral acceleration Sa corresponding to the calculated effective period from the smoothed response spectrum.

$$S_a = \frac{S_a(T_e)}{B} \quad (5.4)$$

Step 8: Calculate new design displacement (D_d) for the isolator.

$$D_d = S_a g \frac{{T_e}^2}{4\pi^2} \quad (5.5)$$

Step 9: Continue the iteration until the difference between the new and previous design displacements is smaller than the tolerance level.

Obtained effective period of the structure (T_e) and the damping reduction factor of structure (B) properties from equivalent linear analysis are shown in table below.

Table 5.1 Result of Equivalent Linear Analysis

	Equivalent Linear Properties Of The Seismic Isolation System			
ANALYSIS NUMBER	**Te (sec)**	**ζe**	**B**	**Dd(cm)**
1	3,08	0,14	1,35	54,92
2	3,79	0,18	1,47	61,83
3	4,30	0,22	1,56	66,50
4	4,12	0,10	1,23	80,70
5	3,45	0,26	1,64	50,85
6	3,79	0,18	1,47	61,83
7	3,79	0,18	1,47	61,83
8	3,79	0,18	1,47	61,83
9	3,79	0,18	1,47	61,83
10	3,79	0,18	1,47	61,83
11	3,00	0,35	1,79	20,18
12	4,07	0,11	1,28	114,84
13	4,20	0,08	1,15	176,38
14	3,53	0,24	1,60	40,90
15	3,90	0,16	1,41	77,11
16	4,12	0,1	1,23	80,70
17	3,79	0,183	1,47	61,83
18	3,45	0,258	1,64	50,85
19	3,00	0,348	1,79	20,18
20	4,07	0,114	1,28	114,84
21	4,20	0,079	1,15	176,38

CHAPTER 6

GROUND MOTIONS SELECTION AND SCALING

6.1 Ground Motion Selection

Effective period intervals are defined using the calculated effective periods of the structures to facilitate the selection of ground motion sets. Ground motion sets are then generated for each effective period interval and various soil site classes. After determining the effective periods and their intervals for the analysis model domain, ground motions are selected from the PEER database using the midpoint of these intervals. The primary objective of this selection process is to maintain scale factors between 0.2 and 5. To enhance the fit quality of the selected dataset, the PEER's Minimize Mean Square Error (MSE) algorithm is employed. The selected sets of ground motions, categorized by soil site classes A/B, C, and D, are detailed in Tables 6.1, 6.2, and 6.3, respectively.

Table 6.1 Motions Selected for the Soil Site Class A/B

GM ID	Earthquake	Station Name	Magnitude	R_{rup} (km)
1	Chi-Chi_Taiwan	CHY086	7.62	28.42
2	Chi-Chi_Taiwan	ILA067	7.62	38.82
3	Chi-Chi_Taiwan	TAP067	7.62	97.39
4	Chuetsu-oki_Japan	Joetsu Uragawaraku Kamabucchi	6.8	22.74
5	Iwate_ Japan	AKT017	6.9	33.76
6	Iwate_ Japan	Minase Yuzawa	6.9	21.25
7	Iwate_ Japan	Yuzawa	6.9	25.56

Table 6.2 Motions Selected for the Soil Site Class C

GM ID	Earthquake	Station Name	Magnitude	R_{rup} (km)
1	Loma Prieta	APEEL 9 – Crystal Springs Res	6.93	41.03
2	Northridge-01	Castaic – Old Ridge Route	6.69	20.72
3	Chi-Chi_Taiwan	TCU042	7.62	26.31
4	Cape Mendocino	Loleta Fire Station	7.01	25.91
5	Chuetsu-oki_Japan	Sawa Mizuguti Tokamachi	6.8	27.3
6	Iwate_ Japan	Yuzawa Town	6.9	25.56
7	Darfield_New Zealand	Heathcote Valley Primary School	7	24.47

Table 6.3 Motions Selected for the Soil Site Class D

GM ID	Earthquake	Station Name	Magnitude	R_{rup} (km)
1	Coalinga-01	Parkfield – Fault Zone 7	6.36	31.21
2	Loma Prieta	Hollister City Hall	6.93	27.6
3	Kobe_ Japan	Tadoka	6.9	31.69
4	Chi-Chi_ Taiwan	TCU117	7.62	25.42
5	Chi-Chi_ Taiwan-03	CHY101	6.2	25.3
6	Chuetsu-oki_Japan	Niigata Nishi Kaba District	6.8	29.91
7	El Mayor - Cucapah_Mexico	El Centro Array #10	7.2	20.05

6.2 Ground Motion Scaling

The selected ground motions were scaled to align with the target response spectrum using the PEER Ground Motion Database Program. The target response spectra were derived from smoothed response spectrum functions, which were calculated by incorporating the seismic damping reduction factor (B). The scale factors for the selected ground motions, aimed at minimizing the mean square error between the average acceleration spectra and the target response spectrum within the interval of 0.75 Te to 1.25 Te, are listed in Table 6.4.

Table 6.4 Ground Motion Scale Factors

	Ground Motion Scale Factors						
MODEL NUMBER	GM ID 1	GM ID 2	GM ID 3	GM ID 4	GM ID 5	GM ID 6	GM ID 7
1	3,12	2,58	1,92	1,41	3,80	2,55	2,42
2	2,86	2,36	1,76	1,29	3,48	2,34	2,21
3	2,71	2,24	1,67	1,22	3,30	2,22	2,10
4	3,43	2,83	2,11	1,55	4,18	2,80	2,66
5	2,58	2,13	1,59	1,16	3,14	2,11	2,00
6	2,86	2,36	1,76	1,29	3,48	2,34	2,21
7	2,86	2,36	1,76	1,29	3,48	2,34	2,21
8	2,86	2,36	1,76	1,29	3,48	2,34	2,21
9	2,86	2,36	1,76	1,29	3,48	2,34	2,21
10	2,86	2,36	1,76	1,29	3,48	2,34	2,21
11	1,18	0,97	0,73	0,53	1,43	0,96	0,91
12	4,95	4,09	3,04	2,23	6,02	4,04	3,83
13	7,36	6,08	4,53	3,31	8,96	6,02	5,70
14	3,73	5,38	3,81	3,40	2,62	1,87	1,90
15	3,63	2,09	3,75	1,40	2,51	3,80	2,66
16	3,43	2,83	2,11	1,55	4,18	2,80	2,66
17	2,86	2,36	1,76	1,29	3,48	2,34	2,21
18	2,58	2,13	1,59	1,16	3,14	2,11	2,00
19	1,18	0,97	0,73	0,53	1,43	0,96	0,91
20	4,95	4,09	3,04	2,23	6,02	4,04	3,83
21	7,36	6,08	4,53	3,31	8,96	6,02	5,70

CHAPTER 7

EVALUATION OF DYNAMIC ANALYSIS RESULTS

7.1 Checking The Reliability Of Analysis Results

The model number 21, which will be used to verify the reliability of the analysis results, features a building with 16 stories and 3 bays; it is equipped with a friction pendulum bearing that has a 5-meter radius of sliding surface curvature and a 5% friction coefficient. It is designed for a peak ground acceleration (PGA) of 1.6g and classified under soil site category C. The forces and displacements of link 6 will be assessed to ensure they comply with the desired support conditions. Link 6 is designated as the right corner friction bearing pendulum of model 21, as depicted in Figure 7.1.

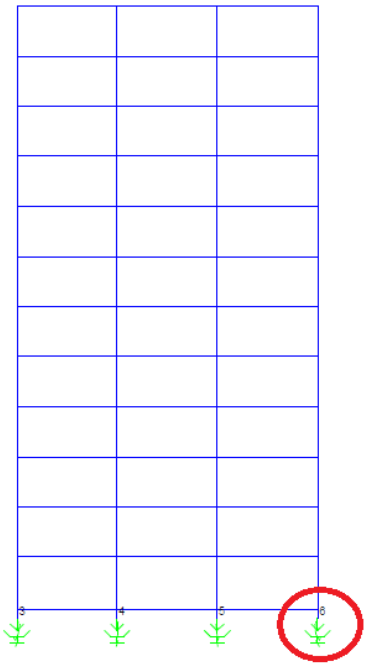

Figure 7.1. Model 21-Link 6

7.1.1.1 Checking The Reliability of Analysis of Uplift Allowed Systems (UAS)

In UAS, upward displacements are expected at corner friction pendulum bearings. This expected structural behaviour can be seen in Figure 7.2.

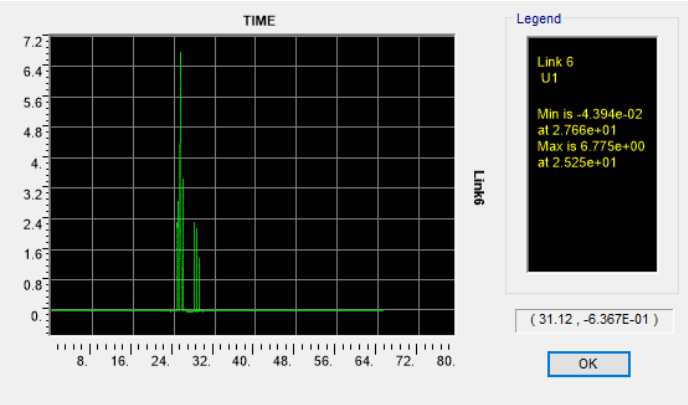

Figure 7.2. Model 21/UAS/Link 6/Time (sec) Vs Vertical Displacement (mm) Graph For Darfield_New Zealand Earthquake Record

Since upward displacement is not restrained in UAS, no tensile force will occur on friction pendulum bearings and this situation is confirmed with Figure 7.3.

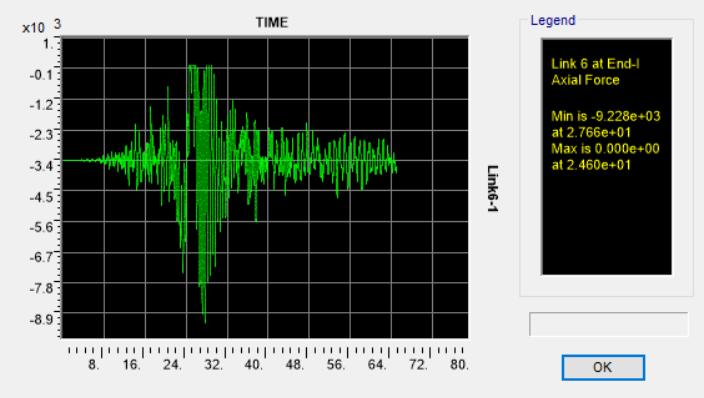

Figure 7.3. Model 21/UAS/Link 6/Time (sec) Vs Axial Force (kN) Graph For Darfield_New Zealand Earthquake Record

7.1.1.2 Checking The Reliability of Analysis of Uplift Restrained Systems (URS)

In URS friction pendulum bearings are restrained along vertical axis so no vertical displacement is observed as shown Figure 7.4.

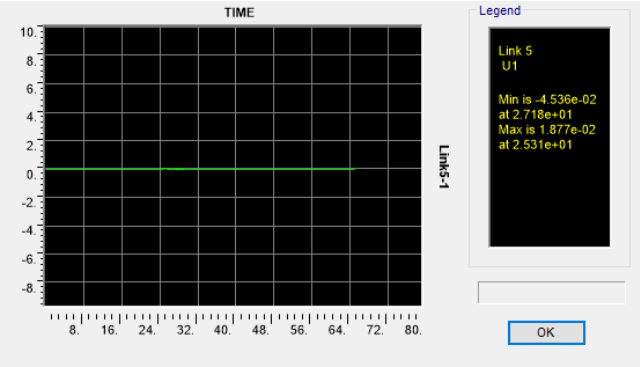

Figure 7.4. Model 21/URS/Link 6/Time (sec) Vs Vertical Displacement (mm) Graph For Darfield_New Zealand Earthquake Record

As a result of restration along vertical axis, tensile forces exist on friction bearing pendulum as shown Figure 7.5.

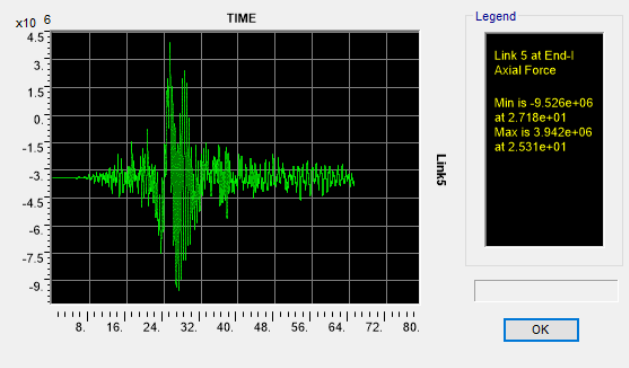

Figure 7.5. Model 21/URS/Link 6/Time (sec) Vs Axial Force (kN) Graph For Darfield_New Zealand Earthquake Record

7.1.1.3 Checking The Reliability of Analysis of Uplift Allowed Impact Modelled Systems (UAIMS)

UAIMS have been adapted from UAS by incorporating an additional damping coefficient, c_{imp}, to account for the impact forces on friction pendulum bearings. As a result, these systems demonstrate support reactions similar to those observed in UAS. Because there are no constraints on upward displacement, such displacements are expected to occur at the corner friction pendulum bearings, resulting in no tensile forces on these bearings. The anticipated structural behaviors are depicted in Figure 7.6 and Figure 7.7, respectively.

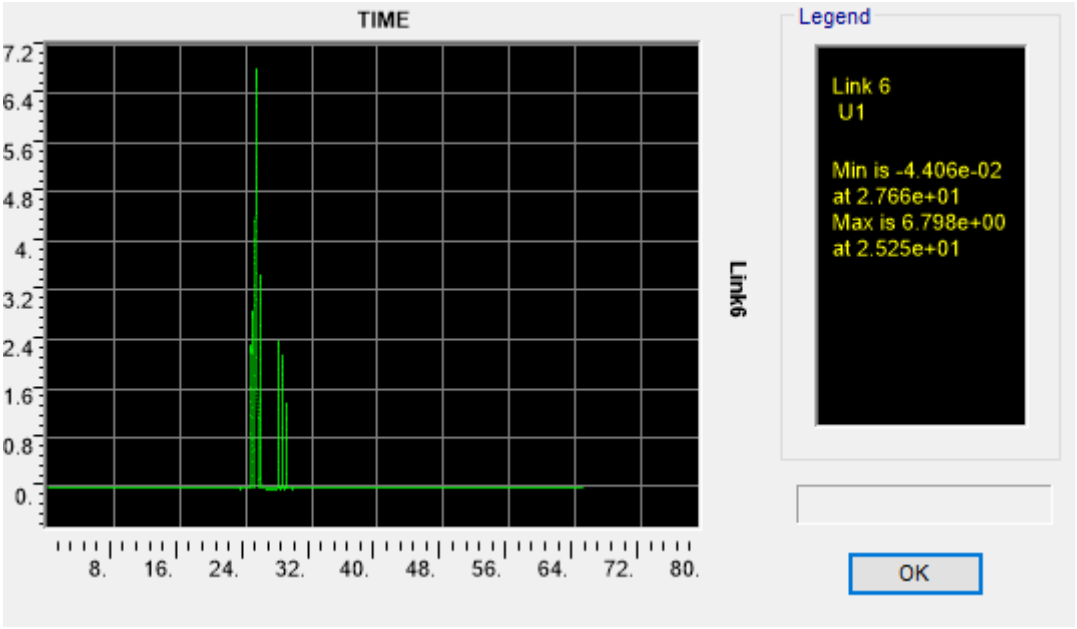

Figure 7.6. Model 21/UAIMS/Link 6/Time (sec) Vs Vertical Displacement (mm) Graph For Darfield_New Zealand Earthquake Record

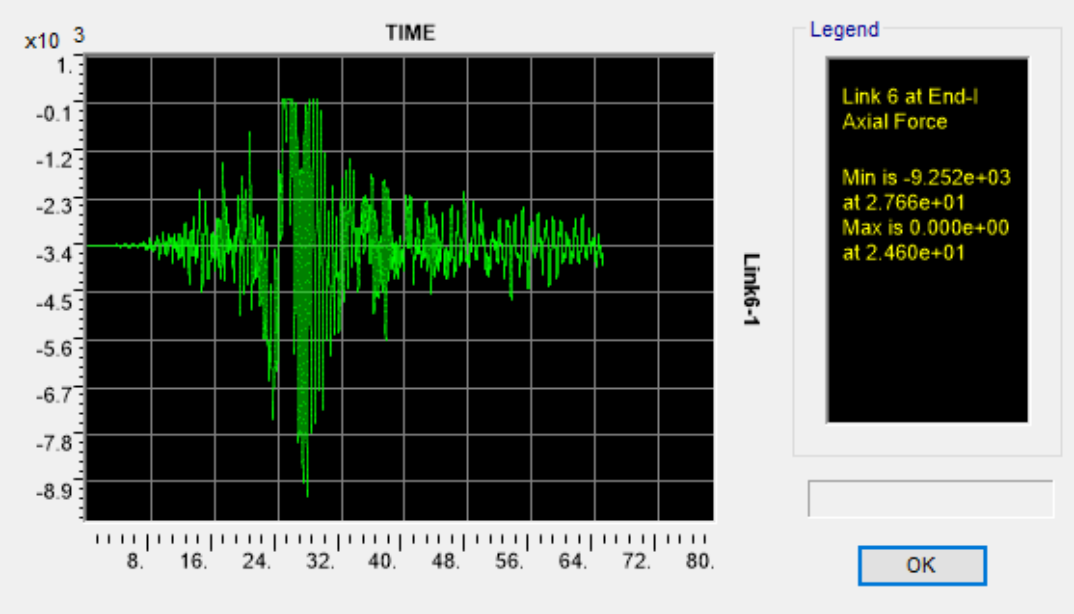

Figure 7.7. Model 21/UAIMS/Link 6/Time (sec) Vs Axial Force (kN) Graph For Darfield_New Zealand Earthquake Record

To assess the reliability of the impact damping effect as defined in analysis models, the base shear forces of Model 21 UAIMS and Model 21 UAS are compared in Figure 7.8. These models incorporate an extremely high damping coefficient c_{imp} due to the impact force on friction pendulum bearings. The comparison reveals that the base shear force in the UAIMS decreases as a result of energy loss caused by the damping effect of the impact.

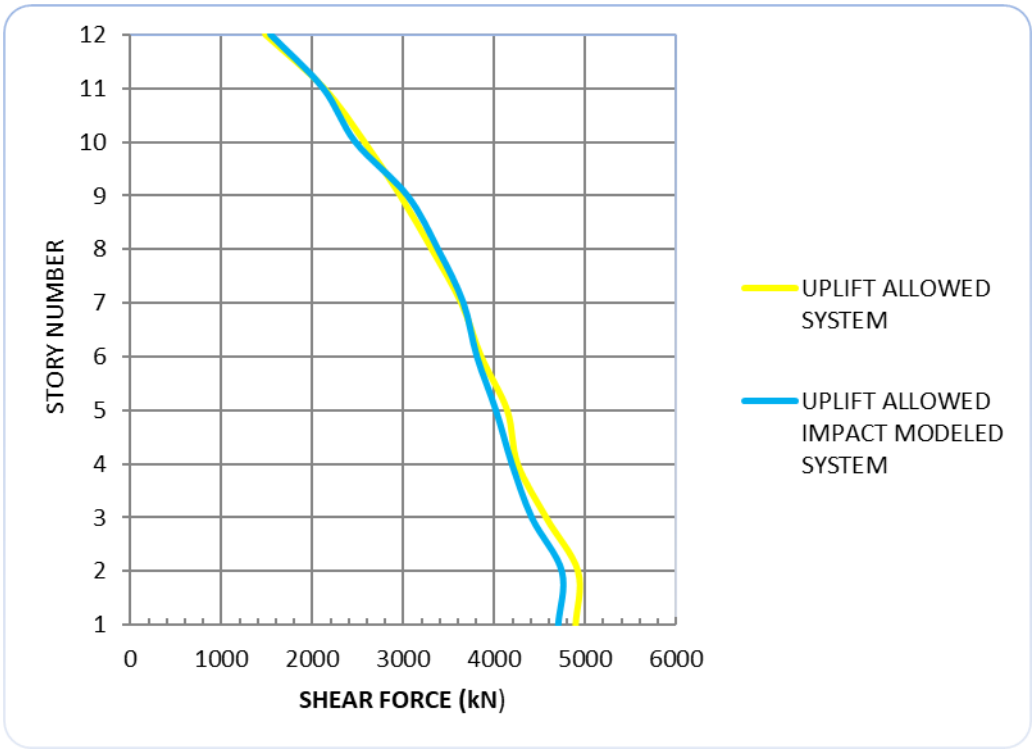

Figure 7.8. Model 21 Shear Force Results Compare Of UAS And UAIMS With Extremely High Damping Coefficient Of Friction Pendulum Bearings (R=5m, μ= %5, Story Nr=12, Bay Nr=3, PGA=1.6g, Soil Type=C)

7.2 Evaluation For 2D Structural Analysis Model With Changing Paramaters

Structural analysis reveals that uplift occurs solely at corner supports. The results, detailed from Appendice A. Figure 8.1 to Figure 8.18, are concisely summarized in Table 7.1. This table includes the maximum uplift displacement for each analysis and compares the base shear force of URS and UAIMS relative to UAS.

Table 7.1 Maximum Uplift Displacement For Each Analysis Model And Base Shear Comparation Of Analysis Results

	Friction Pendulum Bearings Properties		Building Properties										
Model Number	R(m)	μ	Story Number	Bay Number	PGA	Soil Site Classification	UPLIFT (mm)	Base Shear Force for UAS(kN)	Base Shear Force for URS(kN)	Base Shear Force for UAIMS(kN)	% Change Of URS Base Shear According To UAS	% Change Of UAIMS Base Shear According To UAS
1	3	5%	8	5	0,8	C	0,08	3628	3628	3618	0,0%	-0,3%
2	5	5%	8	5	0,8	C	0,15	3203	3209	3203	0,2%	0,0%
3	7	5%	8	5	0,8	C	0,15	3064	3066	3063	0,1%	0,0%
4	5	3%	8	5	0,8	C	0,00	-	-	-	-	-
	5	5%	8	5	0,8	C	0,15	3203	3209	3203	0,2%	0,0%
5	5	7%	8	5	0,8	C	0,43	3668	3668	3667	0,0%	0,0%
6	5	5%	4	5	0,8	C	0,00	-	-	-	-	-
	5	5%	8	5	0,8	C	0,15	3203	3209	3203	0,2%	0,0%
7	5	5%	12	5	0,8	C	0,44	4090	4146	4089	1,4%	0,0%
8	5	5%	16	5	0,8	C	1,43	5379	5536	5378	2,9%	0,0%
9	5	5%	8	3	0,8	C	0,20	1798	1798	1798	0,0%	0,0%
	5	5%	8	5	0,8	C	0,15	3203	3209	3202	0,2%	0,0%
10	5	5%	8	7	0,8	C	0,13	4304	4327	4304	0,5%	0,0%
11	5	5%	8	5	0,4	C	0,00	-	-	-	-	-
	5	5%	8	5	0,8	C	0,15	3203	3209	3202	0,2%	0,0%
12	5	5%	8	5	1,2	C	0,14	4304	4327	4304	0,5%	0,0%
13	5	5%	8	5	1,6	C	0,78	5463	5552	5458	1,6%	-0,1%
14	5	5%	8	5	0,8	A/B	0,09	3051	3055	3043	0,1%	-0,3%
	5	5%	8	5	0,8	C	0,15	3203	3209	3202	0,2%	0,0%

Benchmark
Changing Properties

EXTREME CASES

	Friction Pendulum Bearings Properties		Building Properties									
MODEL NUMBER	R(m)	μ	Story Number	Bay Number	PGA	Soil Site Classification	UPLIFT (mm)	Base Shear Force For UAS(kN)	Base Shear Force For URS(kN)	Base Shear Force For UAIMS(kN)	% Change Of URS Base Shear According To UAS	% Change Of UAIMS Base Shear According To UAS
16	5	3%	12	3	0,8	C	0,02	2364	2364	2364	0,0%	0,0%
17	5	5%	12	3	0,8	C	0,65	2532	2553	2532	0,8%	0,0%
18	5	7%	12	3	0,8	C	1,61	2972	3101	2956	4,3%	-0,5%
19	5	5%	12	3	0,4	C	0,25	1703	1719	1702	0,9%	-0,1%
	5	5%	12	3	0,8	C	0,65	2532	2553	2532	0,8%	0,0%
20	5	5%	12	3	1,2	C	1,69	3559	3764	3559	5,8%	0,0%
21	5	5%	12	3	1,6	C	3,26	4894	5511	4894	12,6%	0,0%

Results, obtained by evaluating the Table 7.1 are listed below:

- Uplift only occurs at corner supports.
- The radius of curvature of the friction pendulum bearing's sliding surface does not influence uplift.
- Increasing the friction coefficient of the friction pendulum bearing decreases the structure's period, leading to higher spectral acceleration values read from the response spectrum. Consequently, greater horizontal forces impact the structure during an earthquake, increasing the amount of uplift.
- As the Peak Ground Acceleration (PGA) rises, so do the horizontal earthquake forces that cause uplift, thereby increasing the amount of uplift.
- Soil site classes, classified from A/B (hard rock/rock) to E (soft clay soil), affect spectral acceleration values read from the response spectrum. With increasing class severity from A/B to E, more horizontal force affects the structure during an earthquake, thus increasing uplift.
- An increase in the number of stories in a structure and a decrease in the number of bays reduce the structure's inertia against rocking effects, leading to increased uplift.
- For models featuring UAS and uplift-allowed impact modeled systems UAIMS, including extreme cases, base shear forces are nearly identical. Although the base shear forces in UAIMS are expected to be lower than those in UAS due to damping effects during impact, the largest uplift observed in all models is a minimal 3.26 mm, which is unlikely to cause significant damping.
- The percentage change in base shear forces of URS increases with the increase in uplift amount in UAS. When the uplift in UAS is less than 1 mm, the percentage change in URS base shear forces compared to those in UAS is less than 1%, a negligible amount. In 15 out of 21 buildings

examined, this percentage change is less than 1%. The maximum percentage change observed is 12.6% in building model number 21, where the uplift in UAS is also the highest at 3.6 mm. When uplift occurs at a support in UAS, as shown in Figure 7.9, a tension force is generated in URS, as depicted in Figure 7.10 at the same support, resulting in an increase in total base shear force for URS due to the additional shear force at the support.

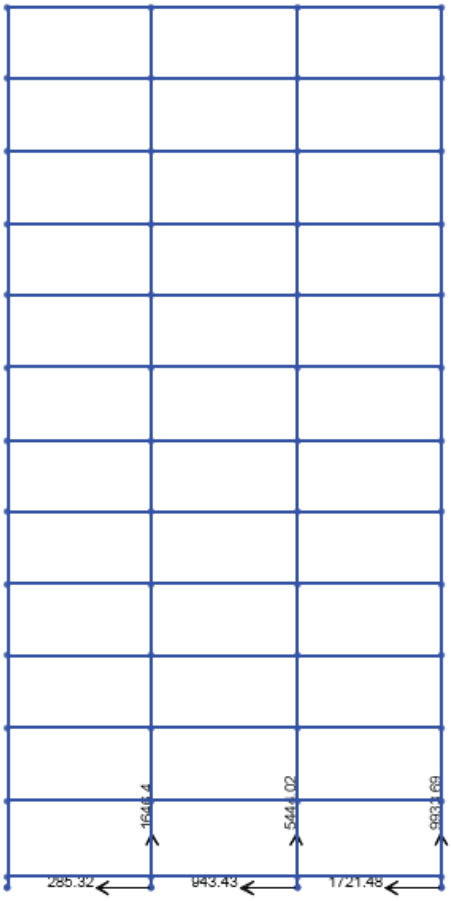

Figure 7.9. Model 21 Uplift Allowed System (UAS) Support Force Results For Northridge-01 Earthquake Record At Time 9.7 Sec. (R=5m, μ= %5, Story Nr=12, Bay Nr=3, PGA=1.6g, Soil Type=C)

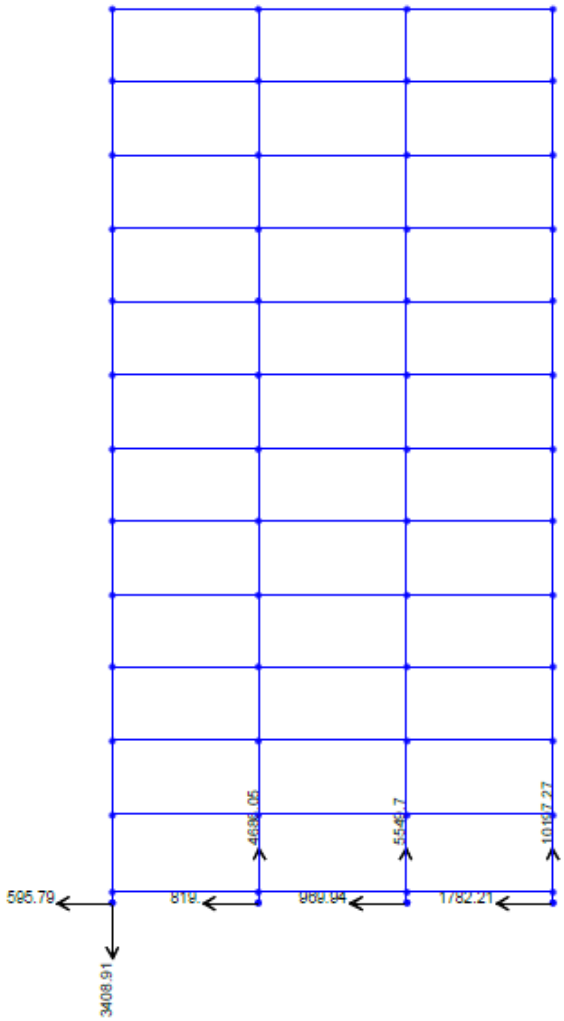

Figure 7.10. Model 21 Uplift Restrained System (URS) Support Force Results For Northridge-01 Earthquake Record At Time 9.7 Sec.(R=5m, μ= %5, Story Nr=12, Bay Nr=3, PGA=1.6g, Soil Type=C)

7.3 Evaluation of Isolator Level Beam's and Shear Wall's Dimension To Impact Effect

For the purpose of evaluation of isolator level beam's and shear wall's dimension to impact effect; Model 8 with 5 bays which is seen in in Figure 7.11 has been revised by adding a shear wall at the middle bay with changing parameter as seen in Figure 7.12.

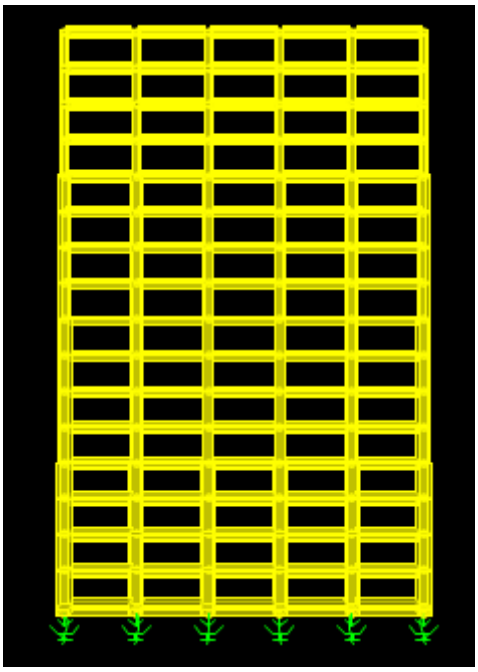

Figure 7.11. Model 8 (R=5m, μ= %5, Story Nr=16, Bay Nr=5, PGA=0.8g, Soil Type=C)

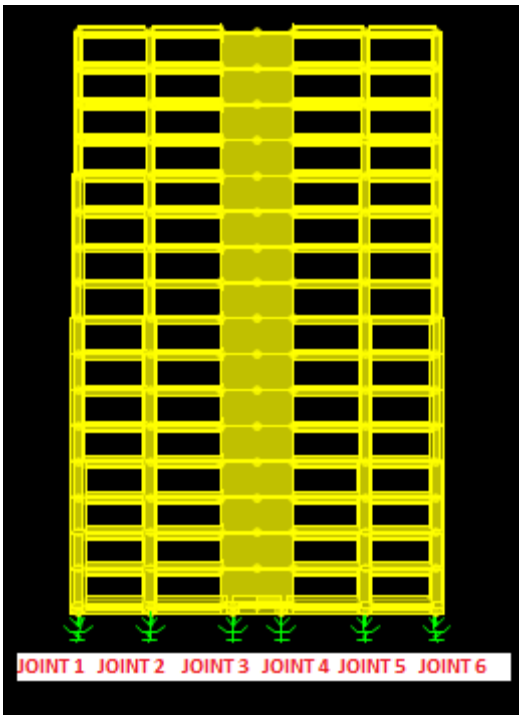

Figure 7.12. Model 8 With Shear Wall At Middle Bay (R=5m, μ= %5, Story Nr=16, Bay Nr=5, PGA=0.8g, Soil Type=C)

Impact of shear wall dimensions on uplift has been shown in Table 7.2.

Table 7.2 Impact Of Shear Wall Dimensions On Uplift

ISOLATOR BEAM DIMENSIONS (CM)	SHEAR WALL DIMENSIONS (CM)	JOINT 1 UPLIFT(mm)	JOINT 2 UPLIFT(mm)	JOINT 3 UPLIFT(mm)	JOINT 4 UPLIFT(mm)	JOINT 5 UPLIFT(mm)	JOINT 6 UPLIFT(mm)
100X100	-	1,45	-	-	-	-	0,29
100X100	400X40	1,40	-	0,23	0,20	-	0,20
100X100	600X40	0,78	-	0,22	0,15	-	0,19
100X100	900X40	-	-	-	-	-	-

Results, obtained by evaluating the Table 7.2 are listed below:

- Since the shear walls are considerably more rigid than the base isolation beams to which they are attached, uplift occurs at the supports at both corners of the shear walls as a result of bending moment .
- With an increase in the cross-section of the wall (sequentially increasing 400x40,600x40,900x40) its overall stiffness or rigidity increases. A more rigid structure is less susceptible to deformation under lateral (sideways) forces, which can help reduce uplift. A larger cross-section also means an increase in the mass of the wall which in turn can decrease uplift.

Impact of isolator base beam dimensions on uplift has been shown in Table 7.3.

Table 7.3 Impact Of Isolator Level Beam Dimensions on Uplift

ISOLATOR BEAM DIMENSIONS (CM)	SHEAR WALL DIMENSIONS (CM)	JOINT 1 UPLIFT(mm)	JOINT 2 UPLIFT(mm)	JOINT 3 UPLIFT(mm)	JOINT 4 UPLIFT(mm)	JOINT 5 UPLIFT(mm)	JOINT 6 UPLIFT(mm)
100X100	600X40	0,78	-	0,22	0,15	-	0,19
150X150	600X40	0,48	-	0,19	0,12	-	-
200X200	600X40	0,32	-	0,14	0,09	-	-
250X250	600X40	0,25	-	0,11	0,06	-	-

The analysis of the Table 7.3. leads to this conclusion below:

Larger cross-sectional dimensions increase the stiffness and strength of the beam, potentially leading to reduced deformation under seismic loads and, consequently, less uplift.

CHAPTER 8

CONCLUSIONS

This study has investigated the impact of uplift in buildings equipped with friction pendulum bearings across 21 models, focusing on UAS, URS, and UAIMS. The thesis also has examined how structural enhancements like the addition of shear walls and the expansion of base isolation beams influence uplift behavior under seismic conditions.

The results demonstrate that uplift is predominantly localized at corner supports, with minimal vertical displacement observed across all models.The base shear forces between UAS and UAIMS are similar, showing that additional damping in UAIMS does not compromise structural performance. However, URS exhibits an increase in base shear forces, up to 12.6% higher than UAS, particularly in scenarios with maximum uplift. This highlights potential challenges when uplift is mechanically restrained, as it can lead to increased structural stresses.It is important to note that while the models analyzed here exhibit very small uplift, systems experiencing relatively larger amounts of uplift could display different behaviors.

Enhancements such as larger shear walls and increased dimensions of base isolation beams significantly improve the building's structural rigidity. These modifications reduce deformation under lateral forces, effectively minimizing the potential for uplift and enhancing the overall seismic resilience of the structure.

In summary, the insights from this study provide a detailed understanding of how various seismic isolation systems respond to seismic forces and how structural

modifications can optimize building performance during earthquakes. These findings offer valuable guidance for improving current designs and implementing effective seismic isolation strategies, emphasizing the need for a balanced design approach to ensure both safety and functional performance in regions susceptible to earthquakes. This study underscores the importance of considering different uplift scenarios in future studies to ensure comprehensive safety and performance assessments.

REFERENCES

[1] G. W. Housner, "The behavior of inverted pendulum structures during earthquakes, "Bulletin of the Seismological Society of America, vol. 53, pp. 403‑417,1963.

[2] D. Kalliontzis and S. Sritharan, "Dynamic response and impact energy loss in controlled rocking members," *Earthquake Engineering and Structural Dynamics*, vol. 49, 2020.

[3] W. Goldsmith, "Impact: The Theory and Physical Behaviour of Colliding Solids," Dover ed., New York: Dover, 2001.

[4] M. Dicleli and S. Buddaram, "Comprehensive evaluation of equivalent linear analysis method for seismic-isolated structures represented by SDOF systems," *Engineering Structures*, vol. 29, no. 8, pp. 1653–1663, 2007.

[5] C. Gosselin and T. Trombetti, "Modeling and seismic response of structures with concrete rocking columns and viscous dampers," *Journal of Structural Engineering*, vol. 136, no. 7, pp. 879–889, 2010.

[6] J. B. Mander and C. T. Cheng, "Earthquake response reduction of buildings by rocking structural systems," Earthquake Engineering & Structural Dynamics, vol. 31, no. 3, pp. 611–629, 2002.

[7] M. E. Rodriguez and E. Miranda, "FEM analyses on seismic responses of rocking structural systems with yielding base plates," *Journal of Earthquake Engineering*, vol. 19, no. 1, pp. 98–123, 2015.

[8] R. Smith, "The response of Veterans Hospital Building 41 in the San Fernando earthquake," Engineering Structures, vol. 4, no. 2, pp. 93–100, 1982.

[9] J. N. Brown and A. J. Kappos, "The interaction of elasticity and rocking in flexible structures allowed to uplift," *Journal of Earthquake Engineering*, vol. 16, no. 8, pp. 1173–1198, 2012.

[10] S. P. Chang and J. X. Zhao, "Dynamic and equivalent static procedures for capacity design of controlled rocking steel-braced frames," *Structural Design of Tall and Special Buildings*, vol. 25, no. 12, pp. 533–550, 2016.

[11] D. Lee and S. W. Han, "Rocking isolation: An effective strategy for limiting forces, permanent displacements, damage, and cost," *International Journal of Structural Stability and Dynamics*, vol. 19, no. 5, pp. 1950034, 2019.
[12] J. C. Matthews and R. Park, "Robust modeling of the rocking problem," *Journal of Structural Engineering*, vol. 138, no. 5, pp. 600–608, 2012.

[13] M. Anderson and V. Bertero, "A half-century of rocking isolation," *Earthquake Spectra*, vol. 30, no. 2, pp. 577–601, 2014.

[14] B. Y. Thompson and J. Penzien, "Seismic response reduction of steel frames with multi-spans by applying rocking structural systems," *Earthquake Engineering & Structural Dynamics*, vol. 35, no. 15, pp. 1857–1877, 2006.

[15] R. A. Harris and G. M. Sabnis, "Experimental study on seismic performance of RC frames with energy-dissipative rocking column system," *Journal of Earthquake Engineering*, vol. 23, no. 3, pp. 467–485, 2019.

[16] E. B. Williamson and D. Mitchell, "Displacement-based analysis and design of rocking structures," *Engineering Structures*, vol. 191, pp. 105–116, 2019.

[17] J. M. Kelly and R. I. Skinner, "The role of rotational inertia in the seismic resistance of free-standing rocking columns and articulated frames," *Journal of Seismology and Earthquake Engineering*, vol. 16, no. 2, pp. 203–215, 2014.

[18] P. Thomas and A. Agrawal, "Seismic response analysis of prestressed concrete rocking frame," *Journal of Structural Engineering*, vol. 147, no. 1, pp. 04020141, 2021.

[19] D. H. Kim and C. Christopoulos, "Seismic performance of a controlled rocking reinforced concrete frame," *Earthquake Engineering & Structural Dynamics*, vol. 46, no. 8, pp. 1285–1304, 2017.

[20] S. Martinez and R. Sterling, "Simplified earthquake analysis of structures with foundation uplift," *Journal of Structural Engineering*, vol. 111, no. 12, pp. 2285–2301, 1985.

APPENDICES

A. Analysis Graphical Results

Twenty-one buildings were selected to assess the rocking effect on friction pendulum bearings. The varying parameters include building story number, building bay number, the curvature radius of the sliding surface on the friction pendulum bearings, friction coefficient, peak ground acceleration, and soil site classification. The buildings were modeled using SAP 2000, a structural analysis and design software. A 2D modeling approach was utilized to effectively evaluate how different structural parameters influence building performance. Graphical results for shear force, moment force, and absolute horizontal displacement are presented from Figure 8.1 to Figure 8.18.

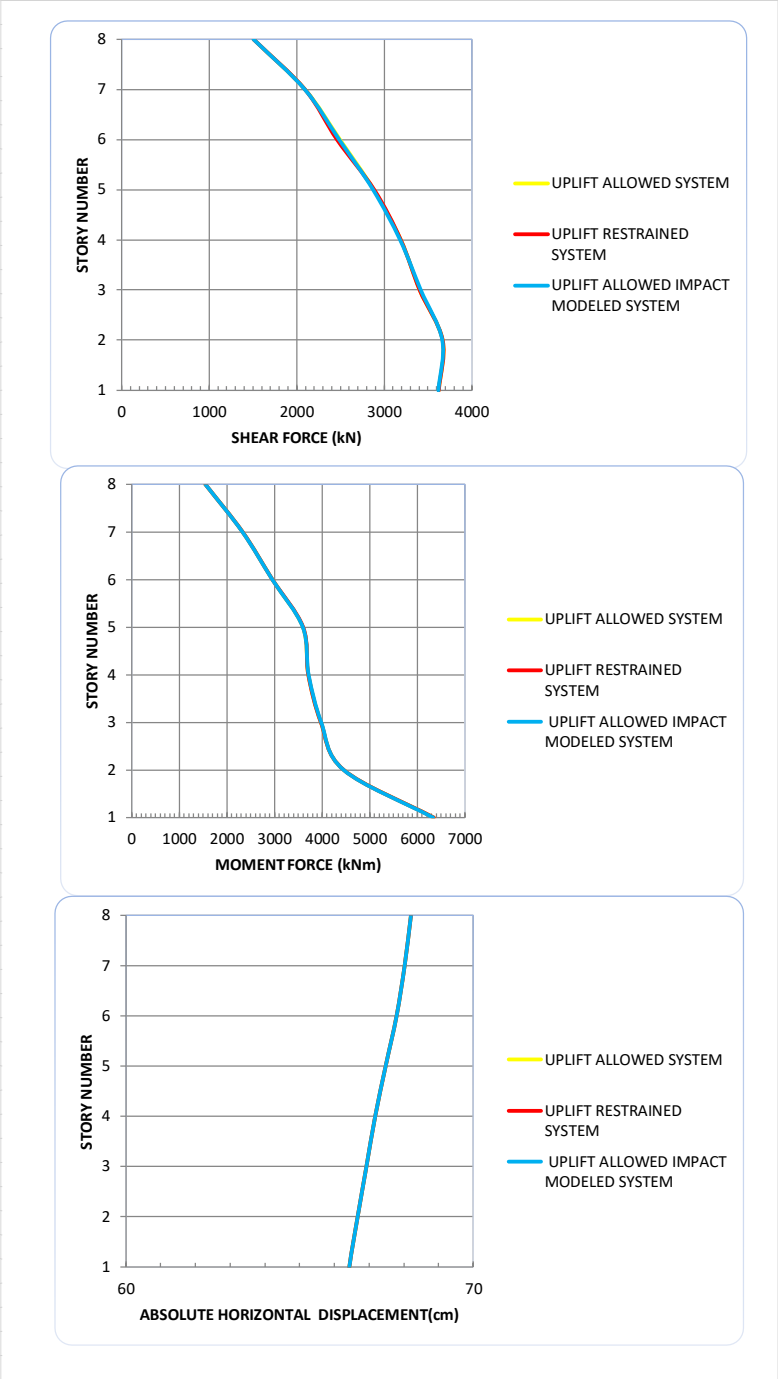

Figure 8.1. Model 1 Analys Results (R=3m, μ= %5, Story Nr=8, Bay Nr=5, PGA=0.8g, Soil Type=C)

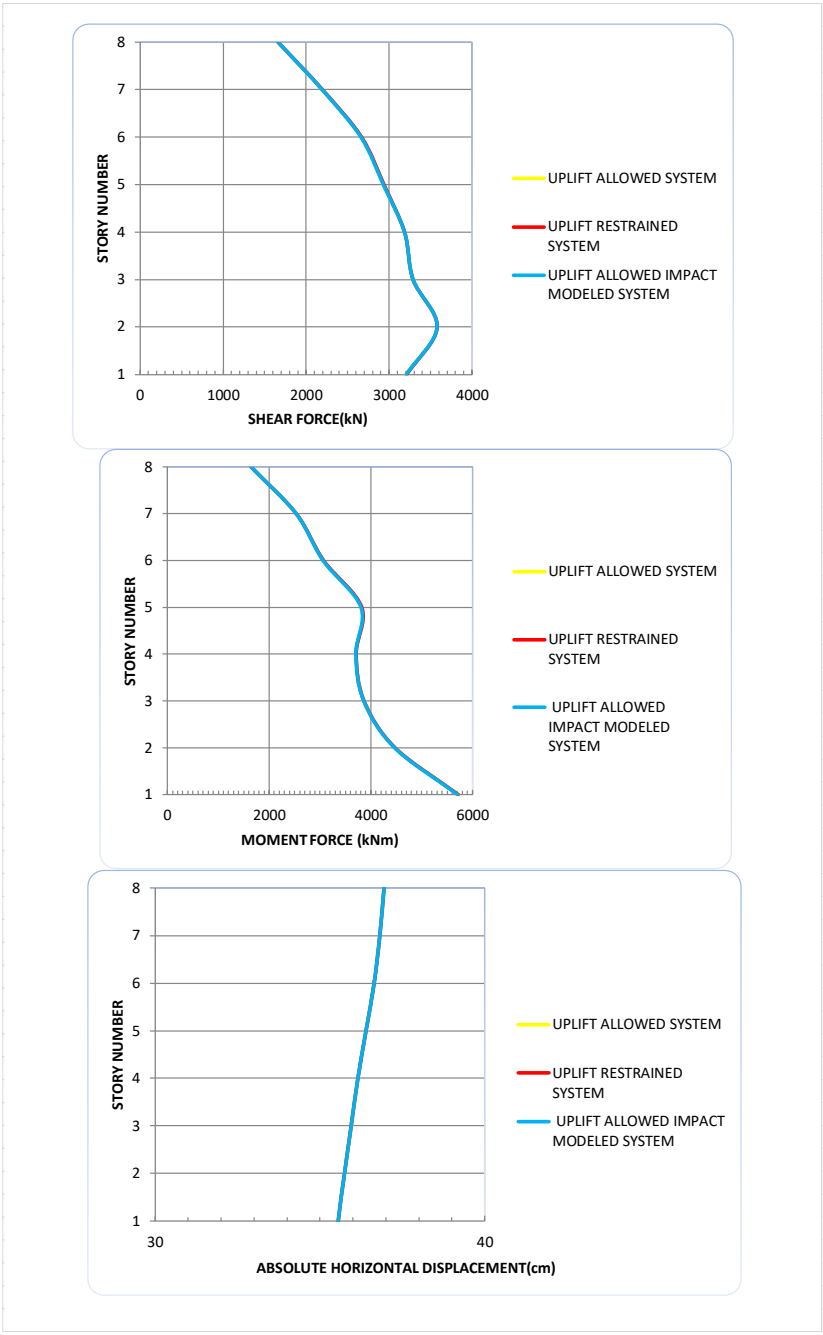

Figure 8.2. Model 2 Analys Results (R=5m, μ= %5, Story Nr=8, Bay Nr=5, PGA=0.8g, Soil Type=C)

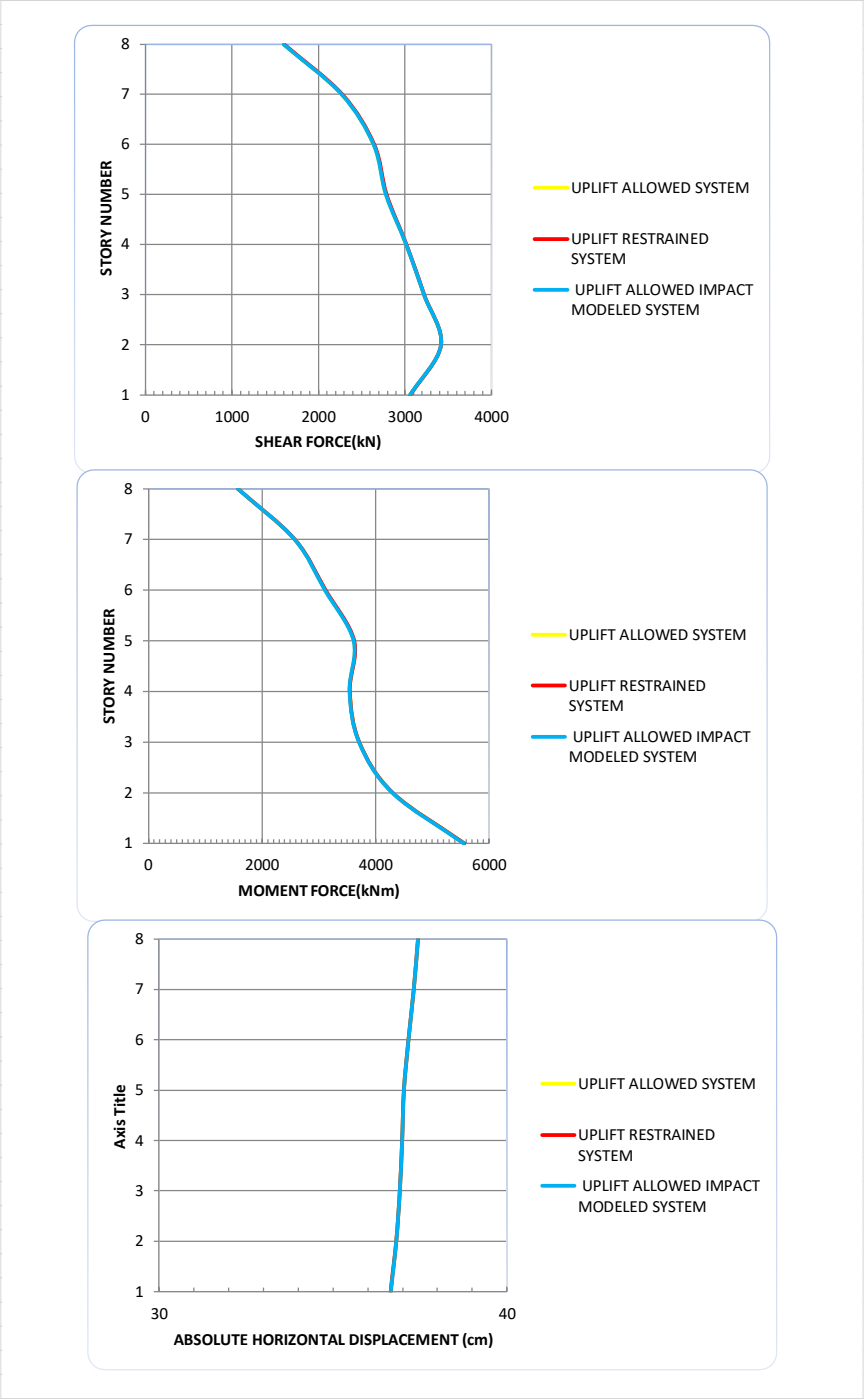

Figure 8.3. Model 3 Analys Results (R=7m, μ= %5, Story Nr=8, Bay Nr=5, PGA=0.8g, Soil Type=C)

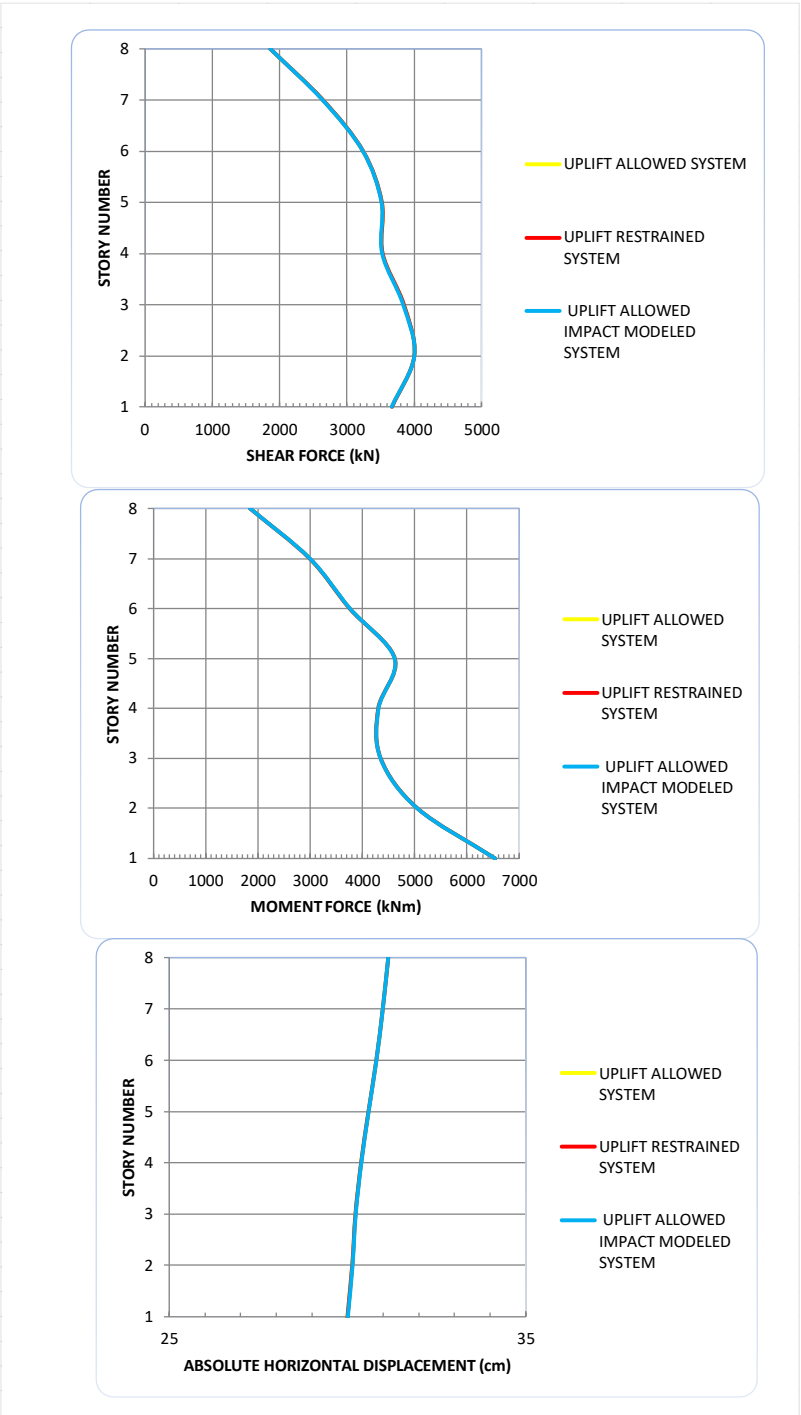

Figure 8.4. Model 5 Analys Results (R=5m, μ= %7, Story Nr=8, Bay Nr=5, PGA=0.8g, Soil Type=C)

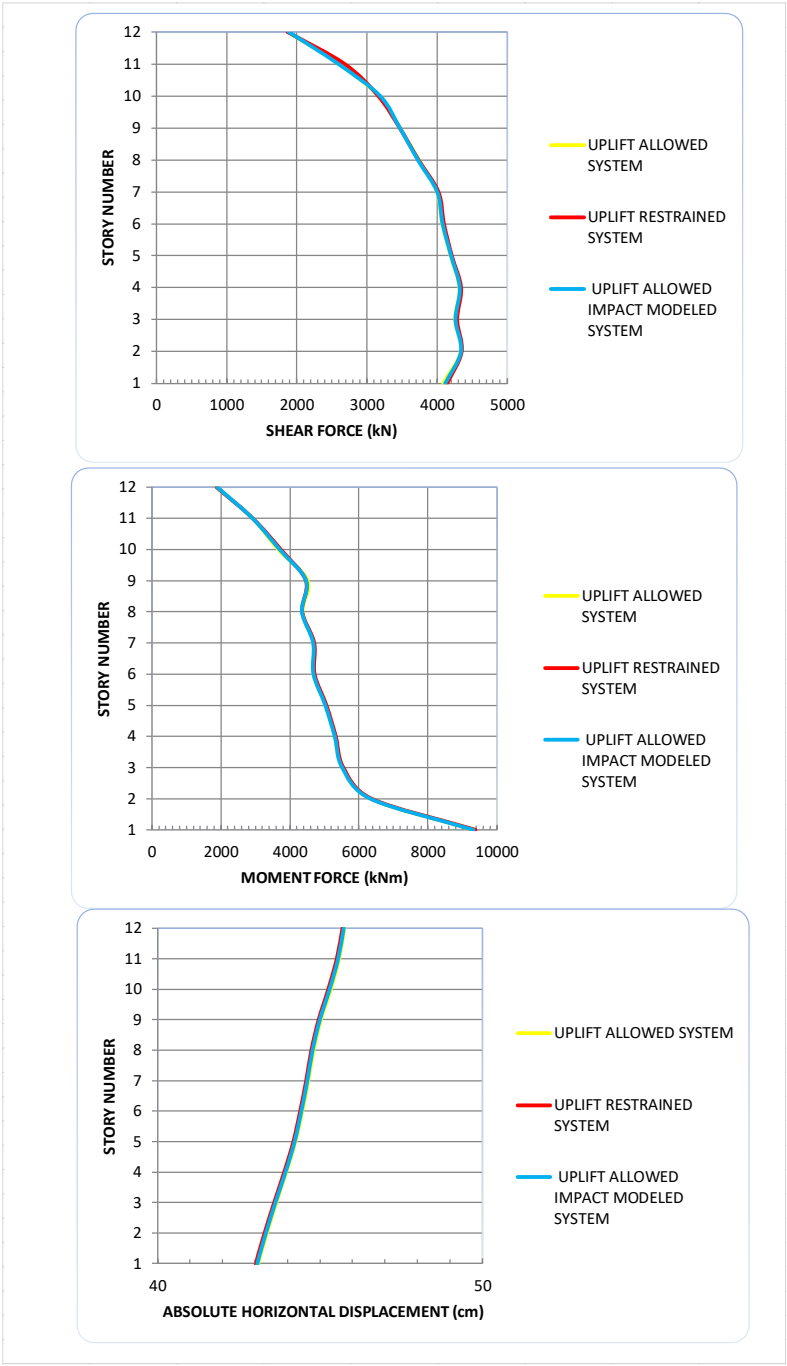

Figure 8.5. Model 7 Analys Results (R=5m, μ= %5, Story Nr=12, Bay Nr=5, PGA=0.8g, Soil Type=C)

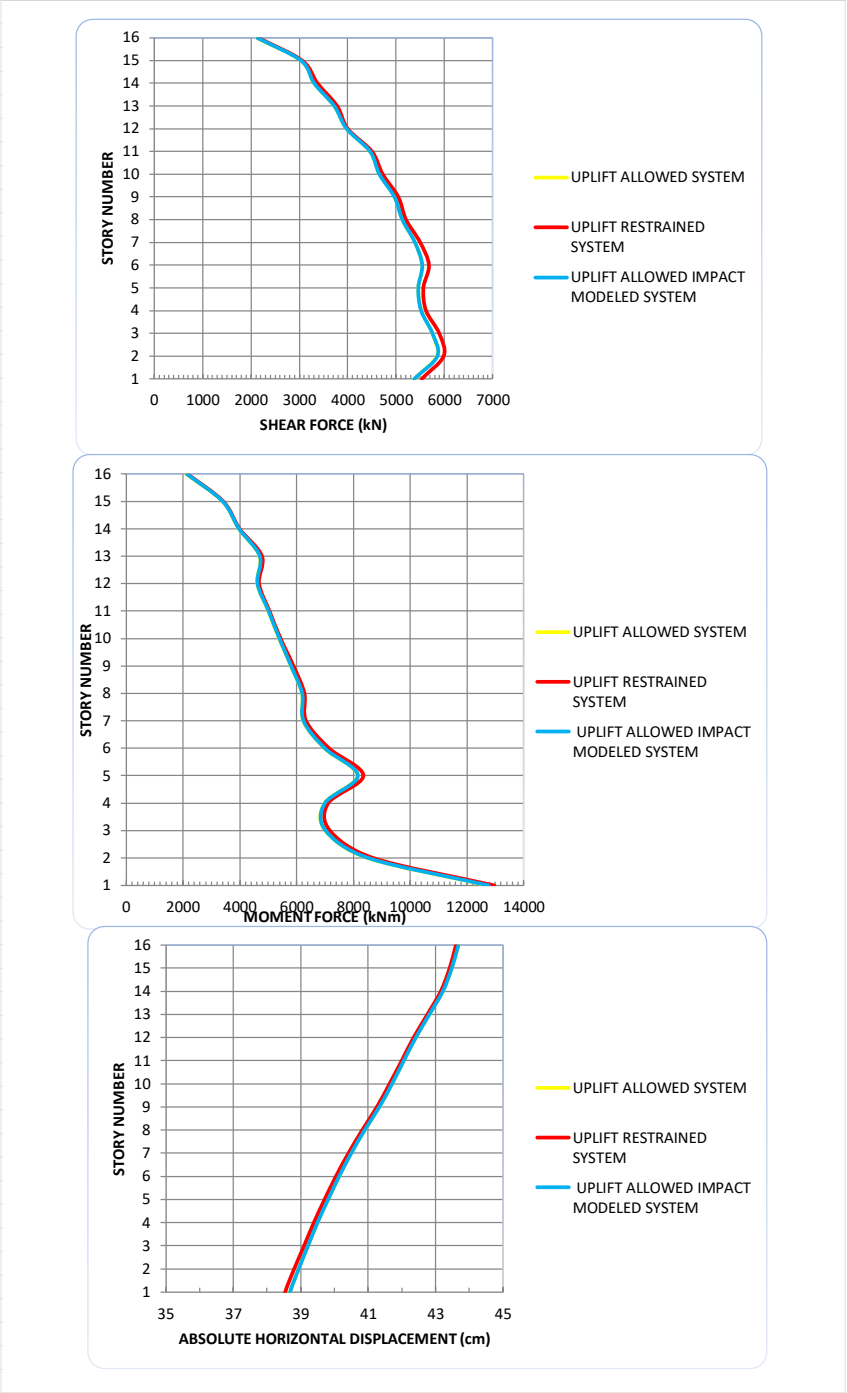

Figure 8.6. Model 8 Analys Results (R=5m, μ= %5, Story Nr=16, Bay Nr=5, PGA=0.8g, Soil Type=C)

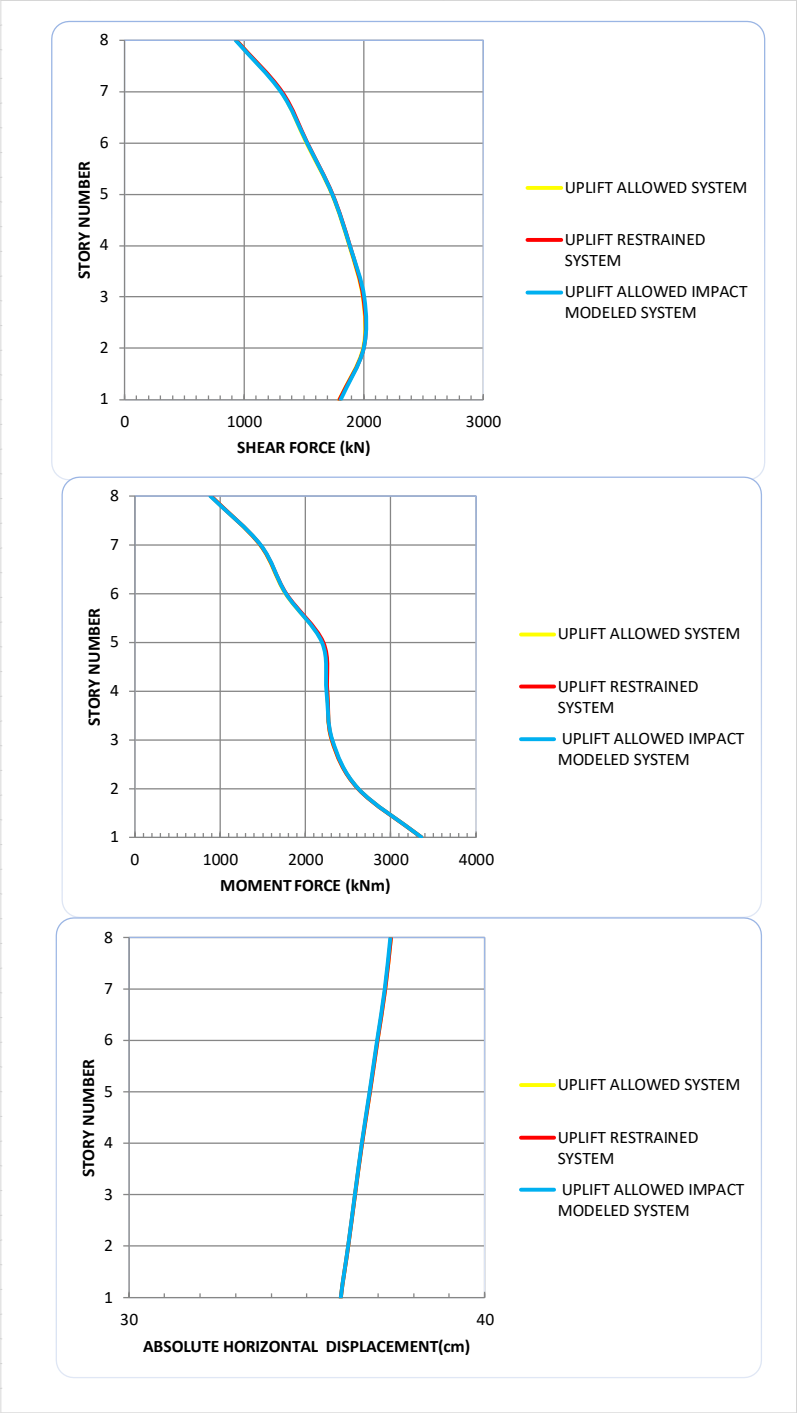

Figure 8.7. Model 9 Analys Results (R=5m, μ= %5, Story Nr=8, Bay Nr=3, PGA=0.8g, Soil Type=C)

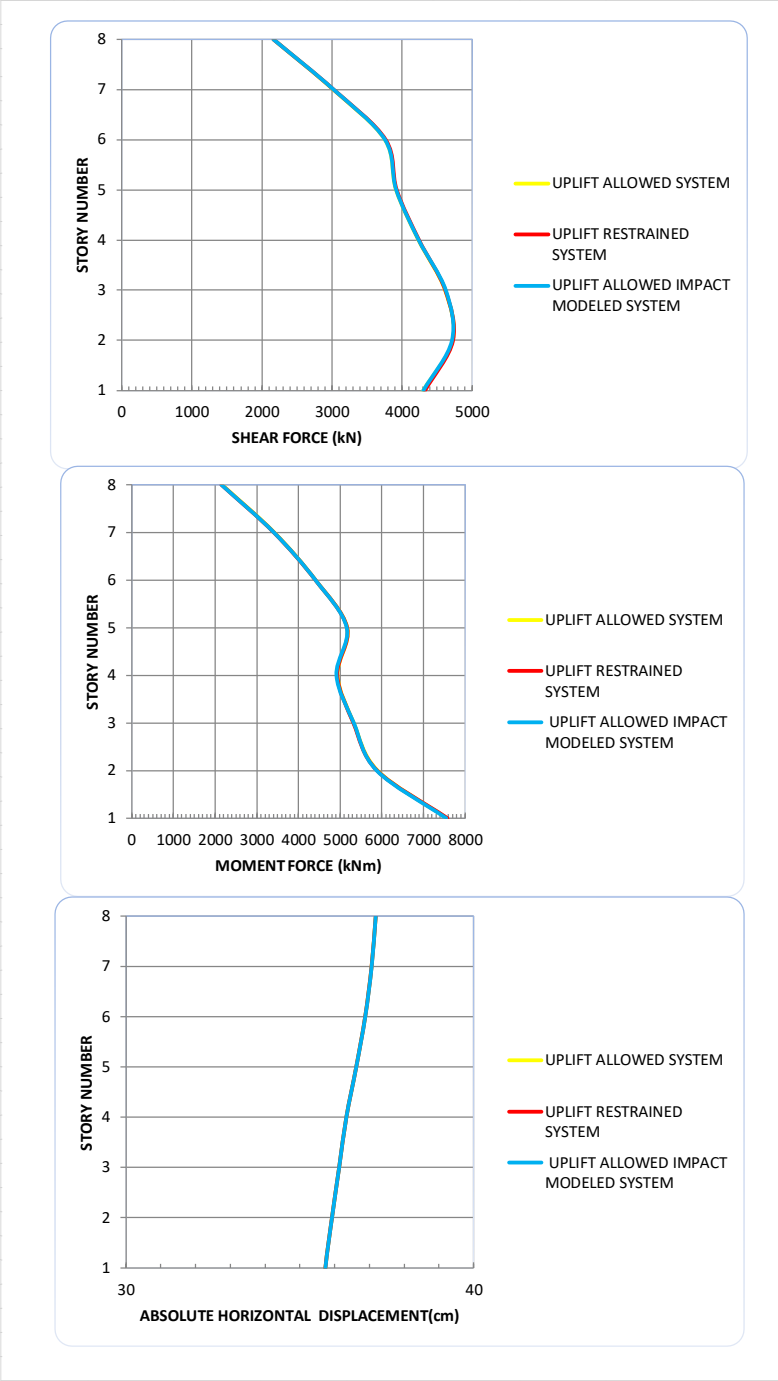

Figure 8.8. Model 10 Analys Results (R=5m, μ= %5, Story Nr=8, Bay Nr=7, PGA=0.8g, Soil Type=C)

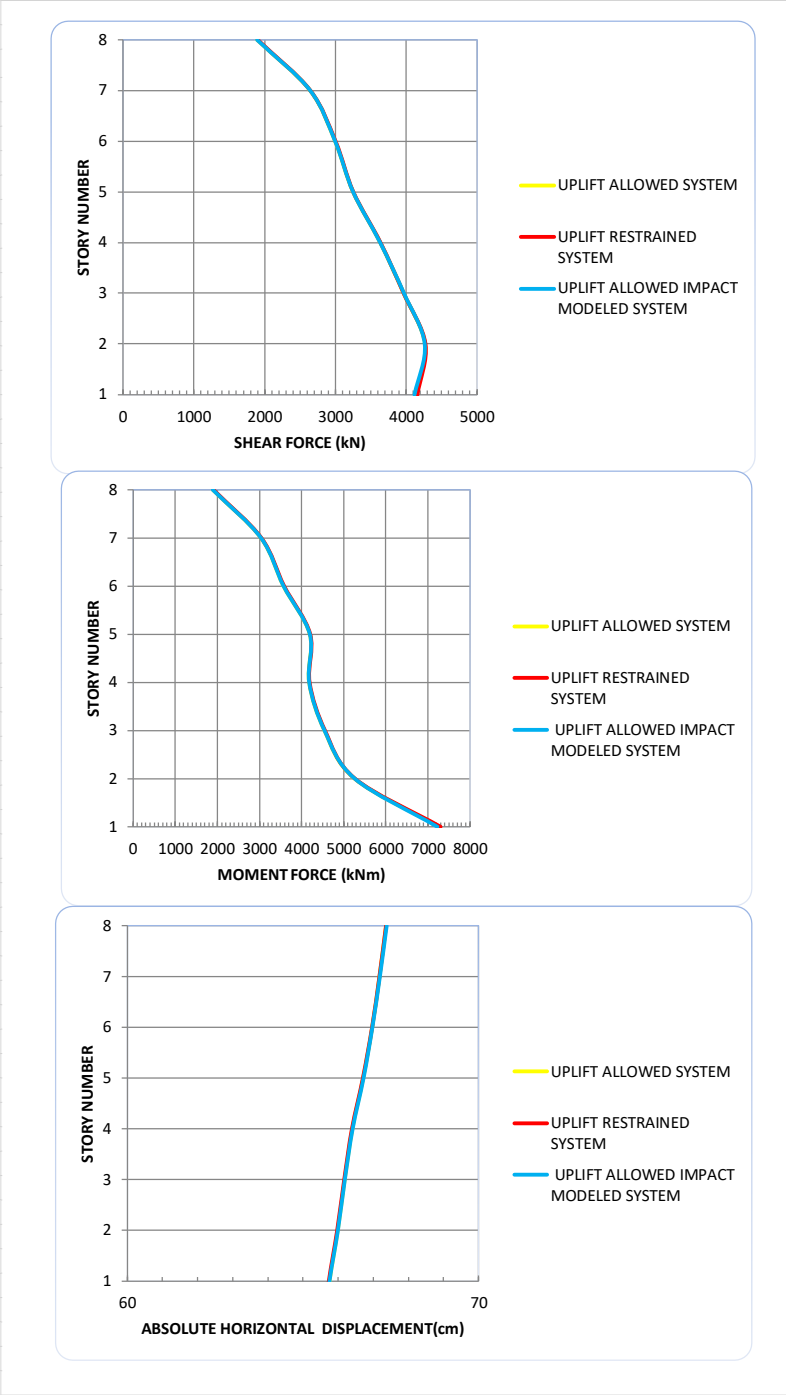

Figure 8.9. Model 12 Analys Results (R=5m, μ= %5, Story Nr=8, Bay Nr=5, PGA=1.2g, Soil Type=C)

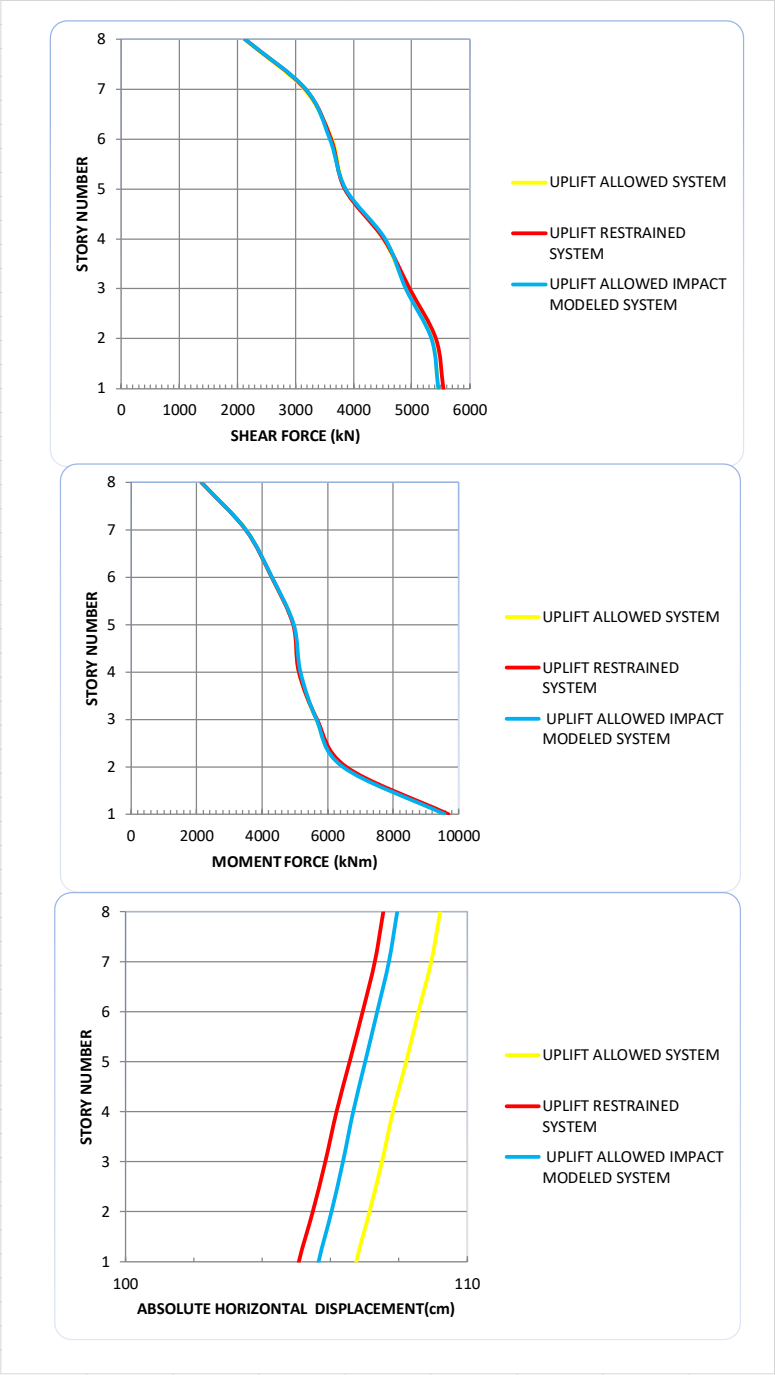

Figure 8.10. Model 13 Analys Results (R=5m, μ= %5, Story Nr=8, Bay Nr=5, PGA=1.6g, Soil Type=C)

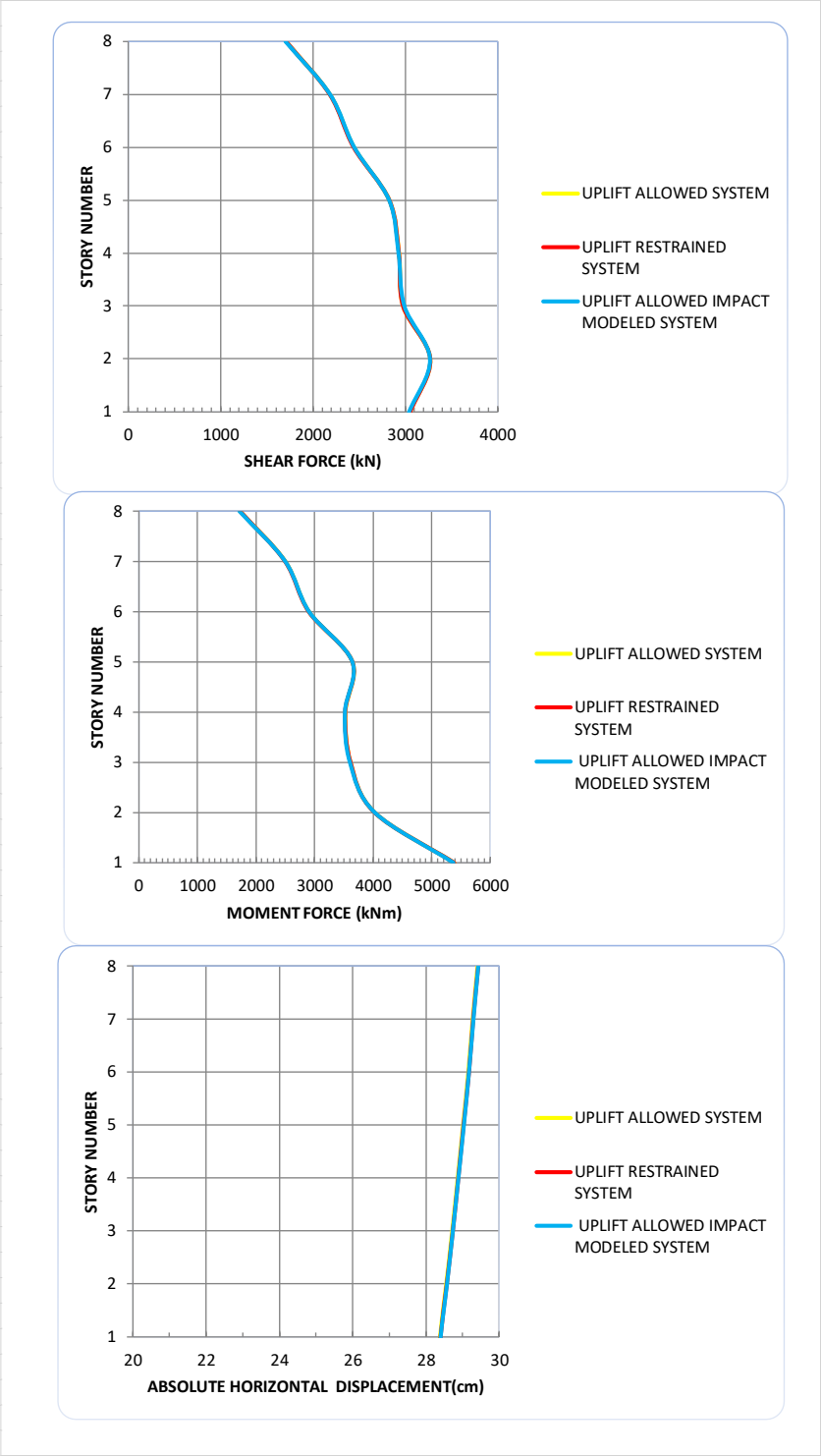

Figure 8.11. Model 14 Analys Results (R=5m, μ= %5, Story Nr=8, Bay Nr=5, PGA=0.8g, Soil Type=A/B)

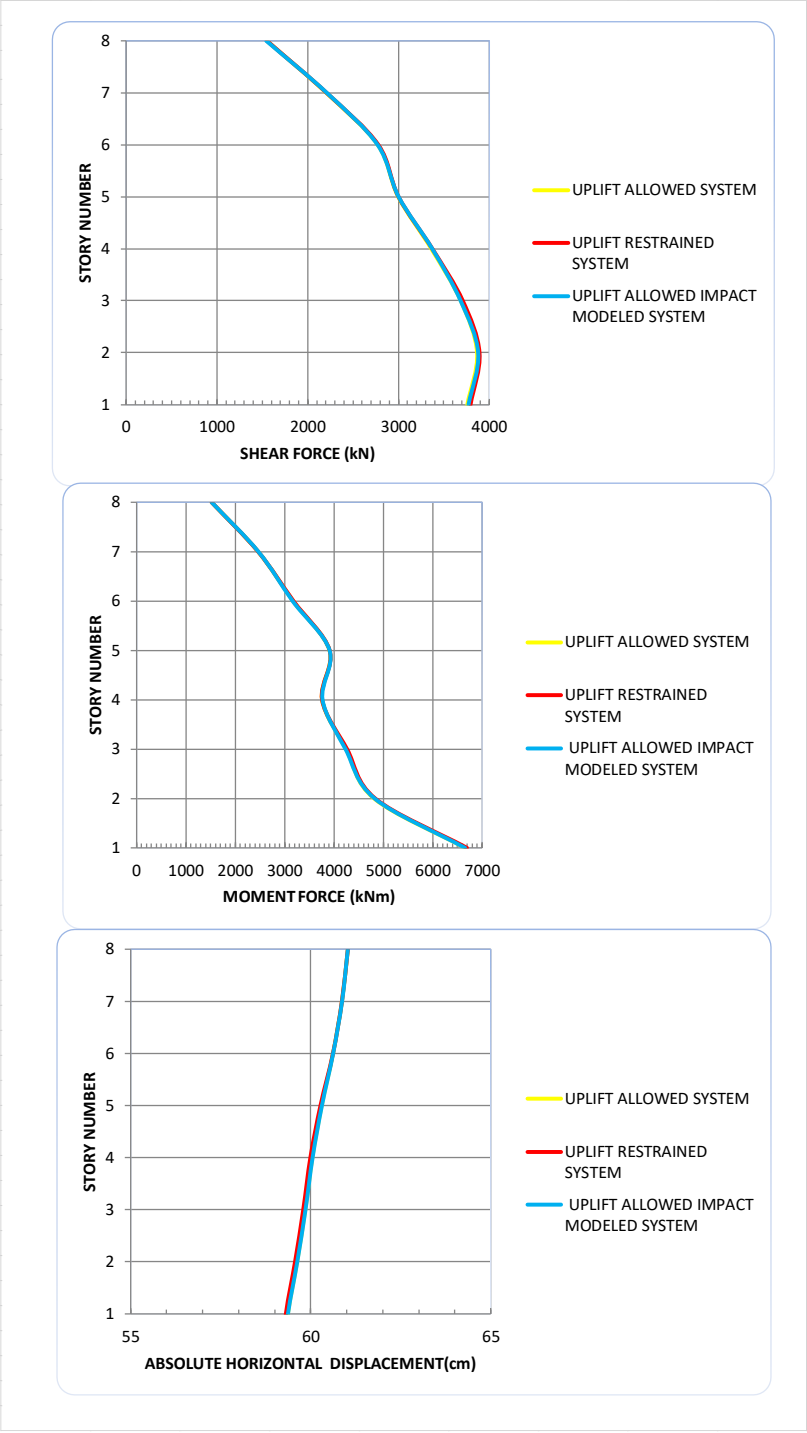

Figure 8.12 Model 15 Analys Results (R=5m, μ= %5, Story Nr=8, Bay Nr=5, PGA=0.8g, Soil Type=D)

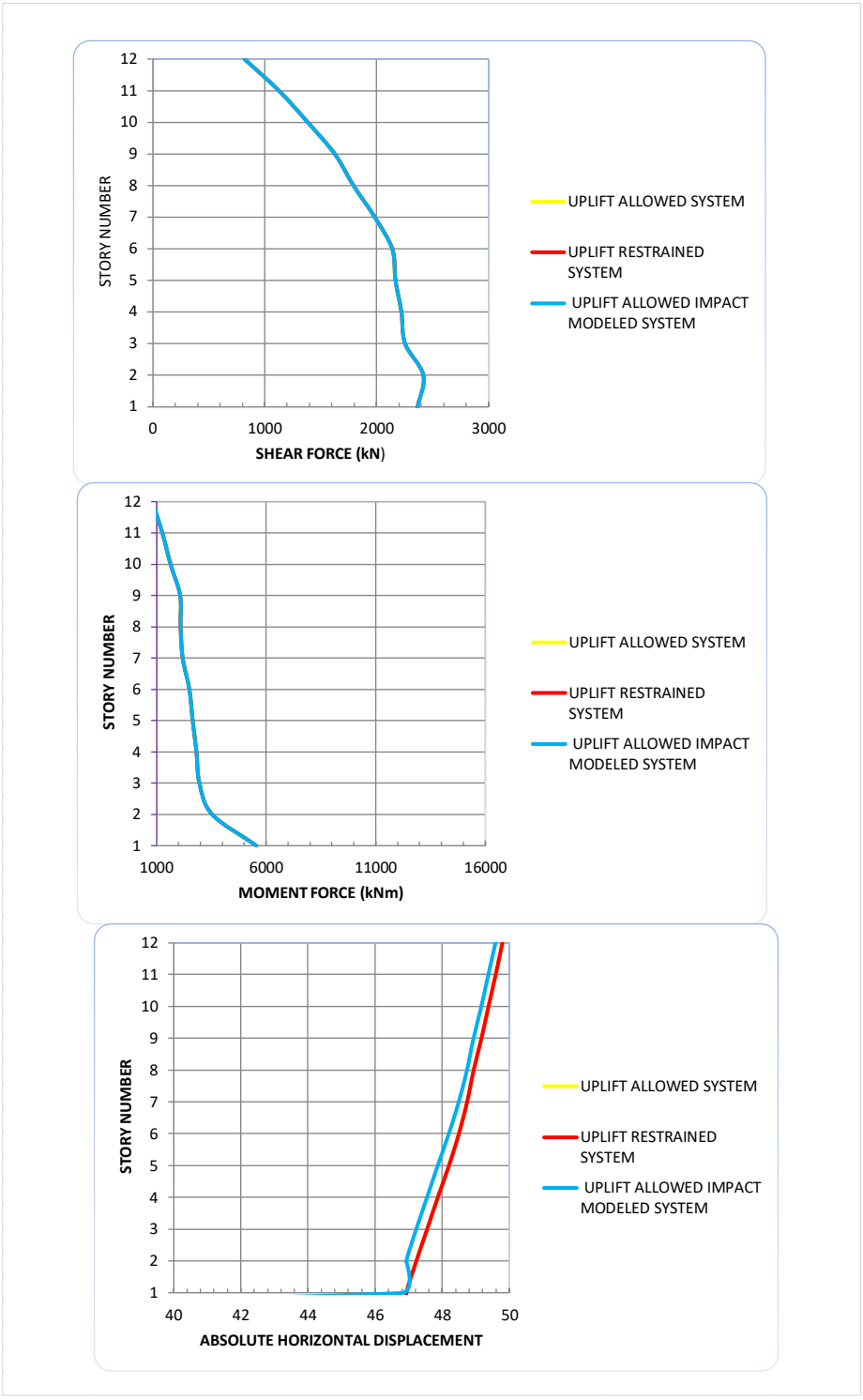

Figure 8.13. Model 16 Analys Results (R=5m, μ= %3, Story Nr=12, Bay Nr=3, PGA=0.8g, Soil Type=C)

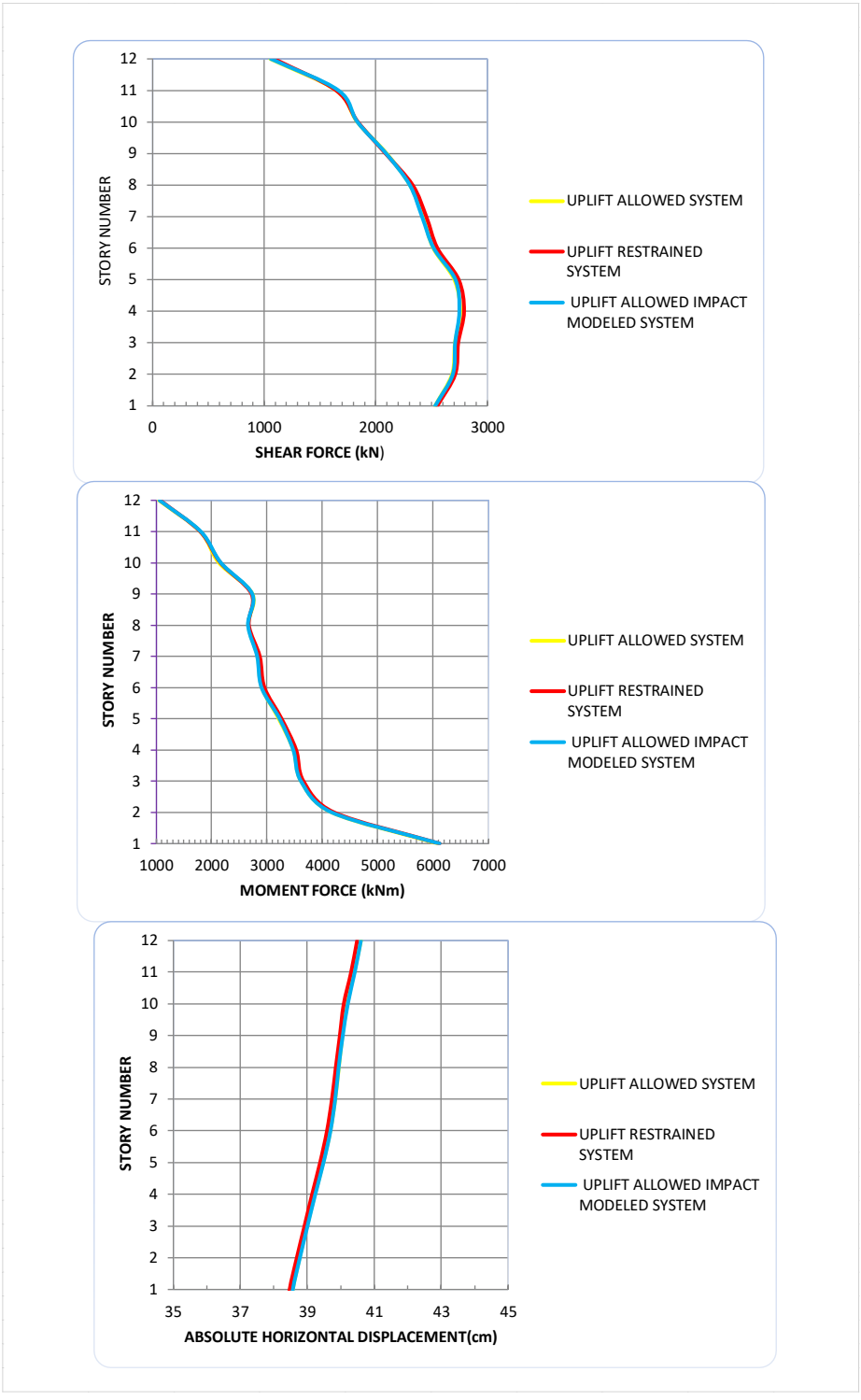

Figure 8.14. Model 17 Analys Results (R=5m, μ= %5, Story Nr=12, Bay Nr=3, PGA=0.8g, Soil Type=C)

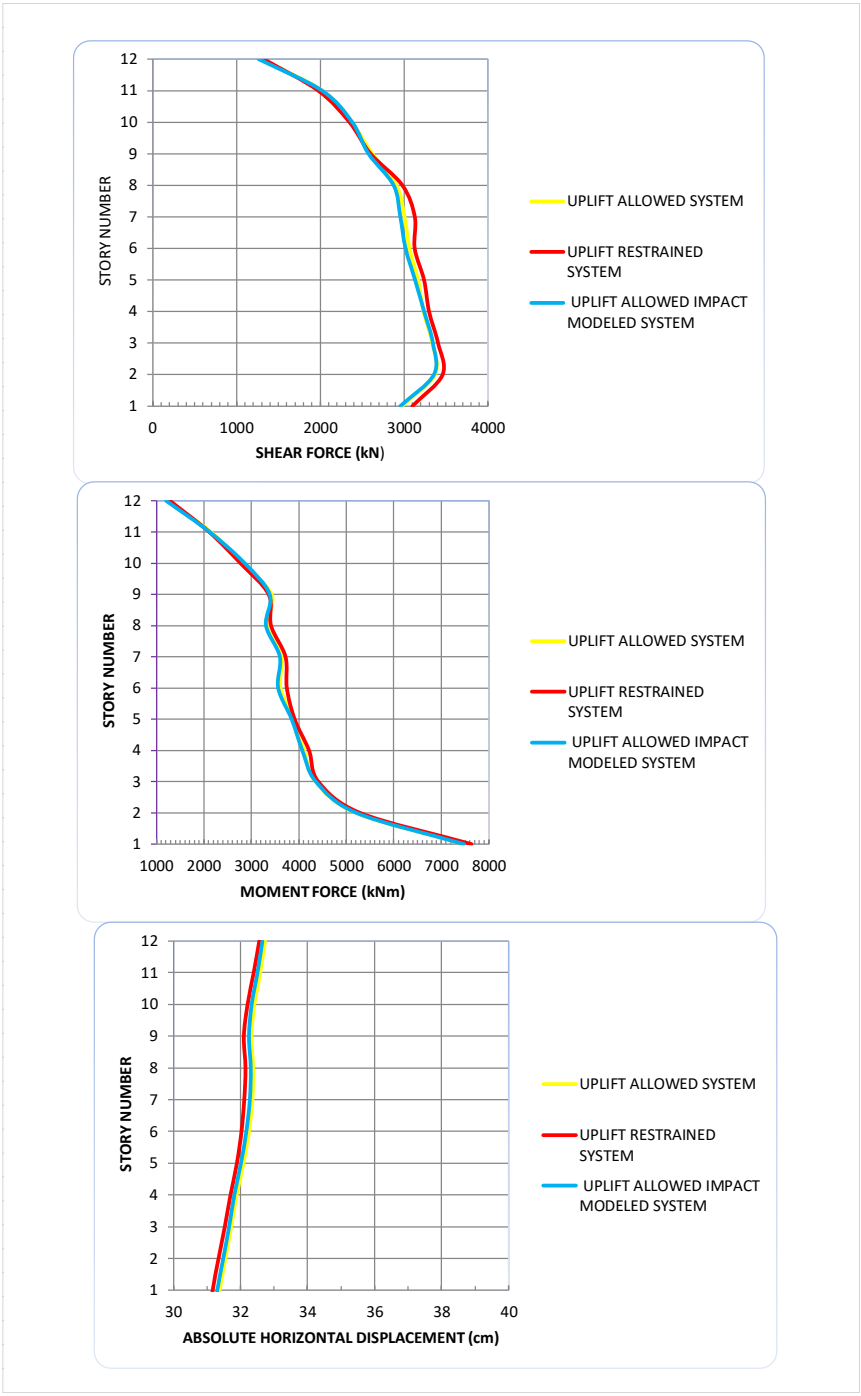

Figure 8.15. Model 18 Analys Results (R=5m, μ= %7, Story Nr=12, Bay Nr=3, PGA=0.8g, Soil Type=C)

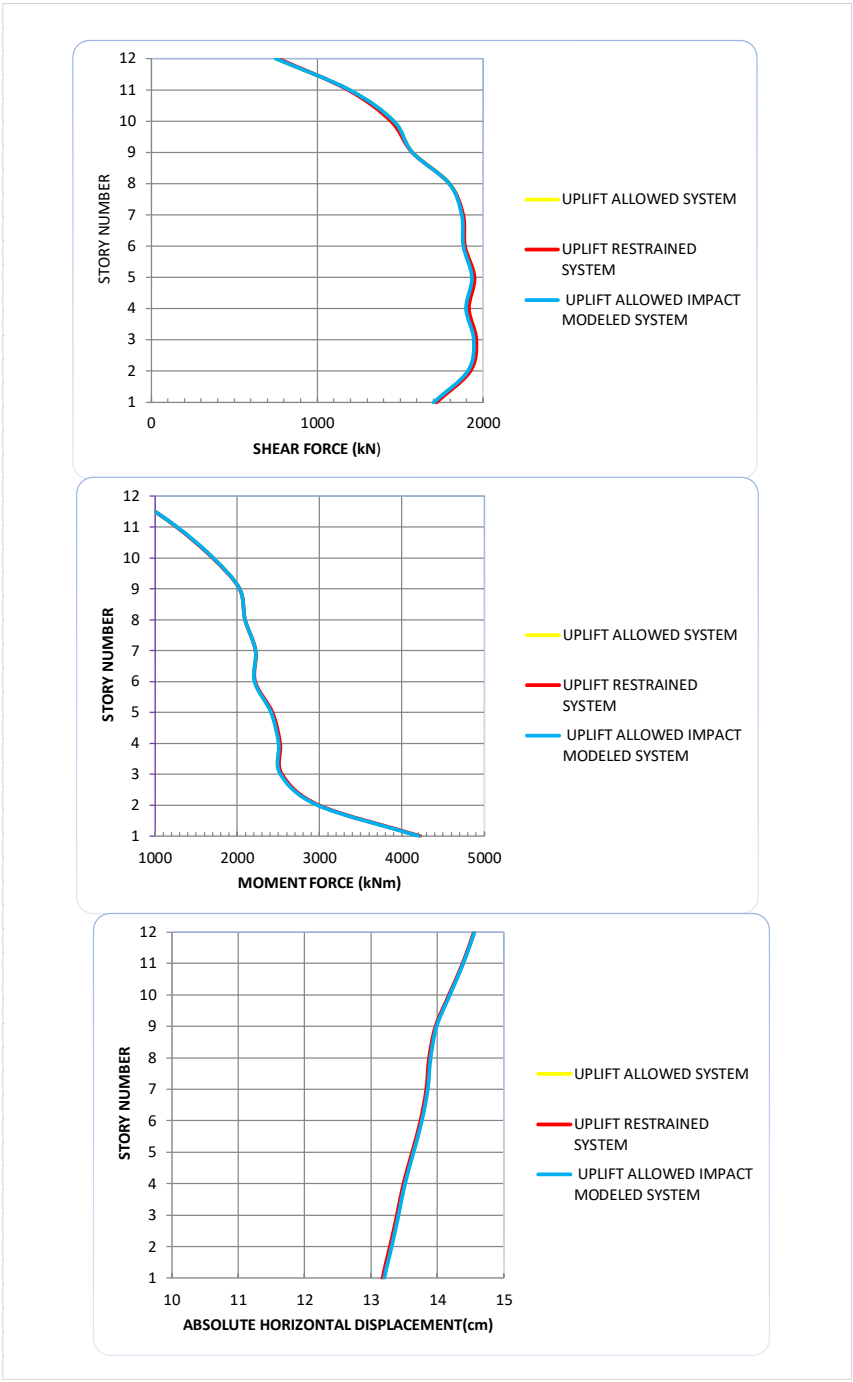

Figure 8.16. Model 19 Analys Results (R=5m, μ= %7, Story Nr=12, Bay Nr=3, PGA=0.4g, Soil Type=C)

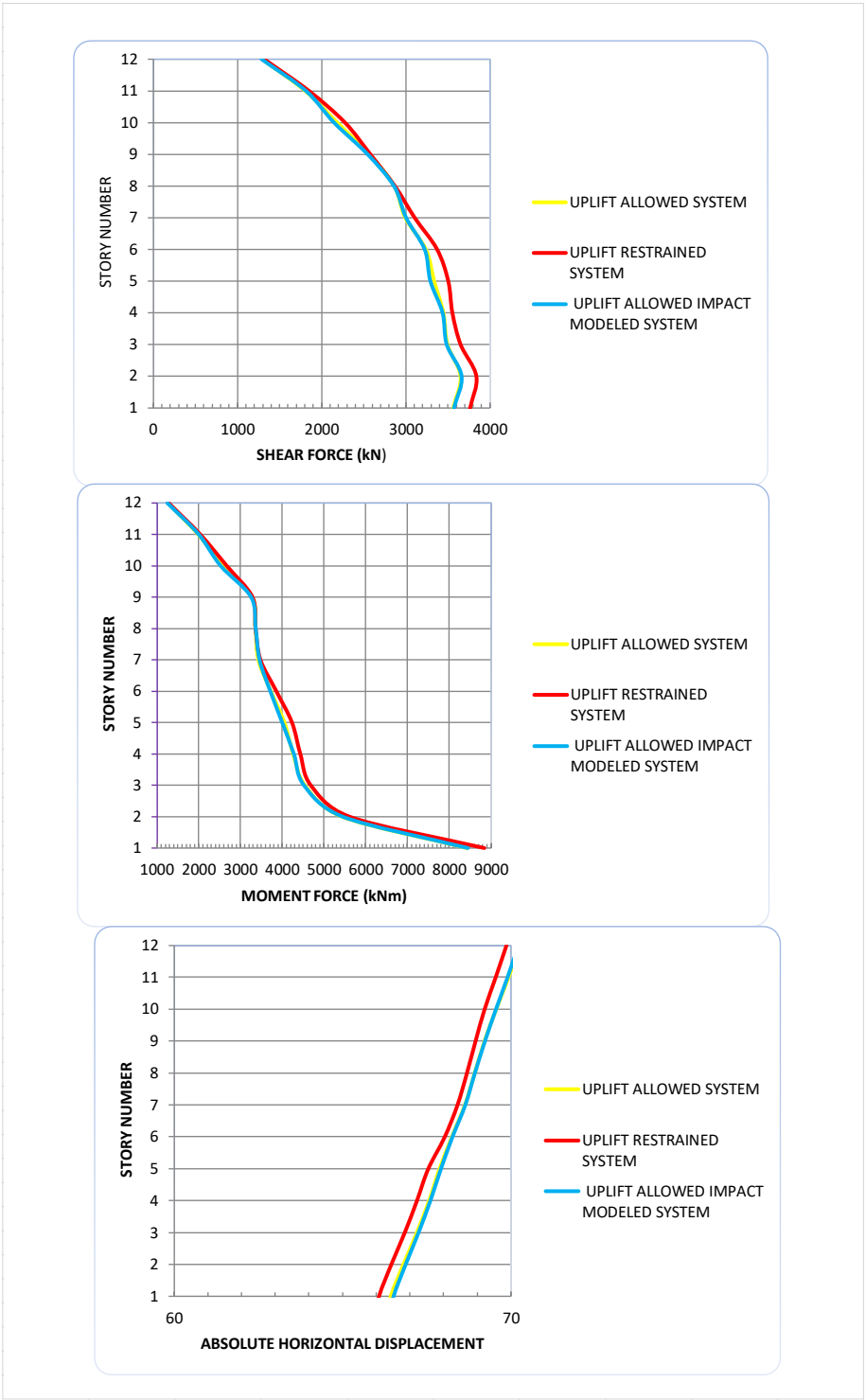

Figure 8.17. Model 20 Analys Results (R=5m, μ= %5, Story Nr=12, Bay Nr=3, PGA=1.2g, Soil Type=C)

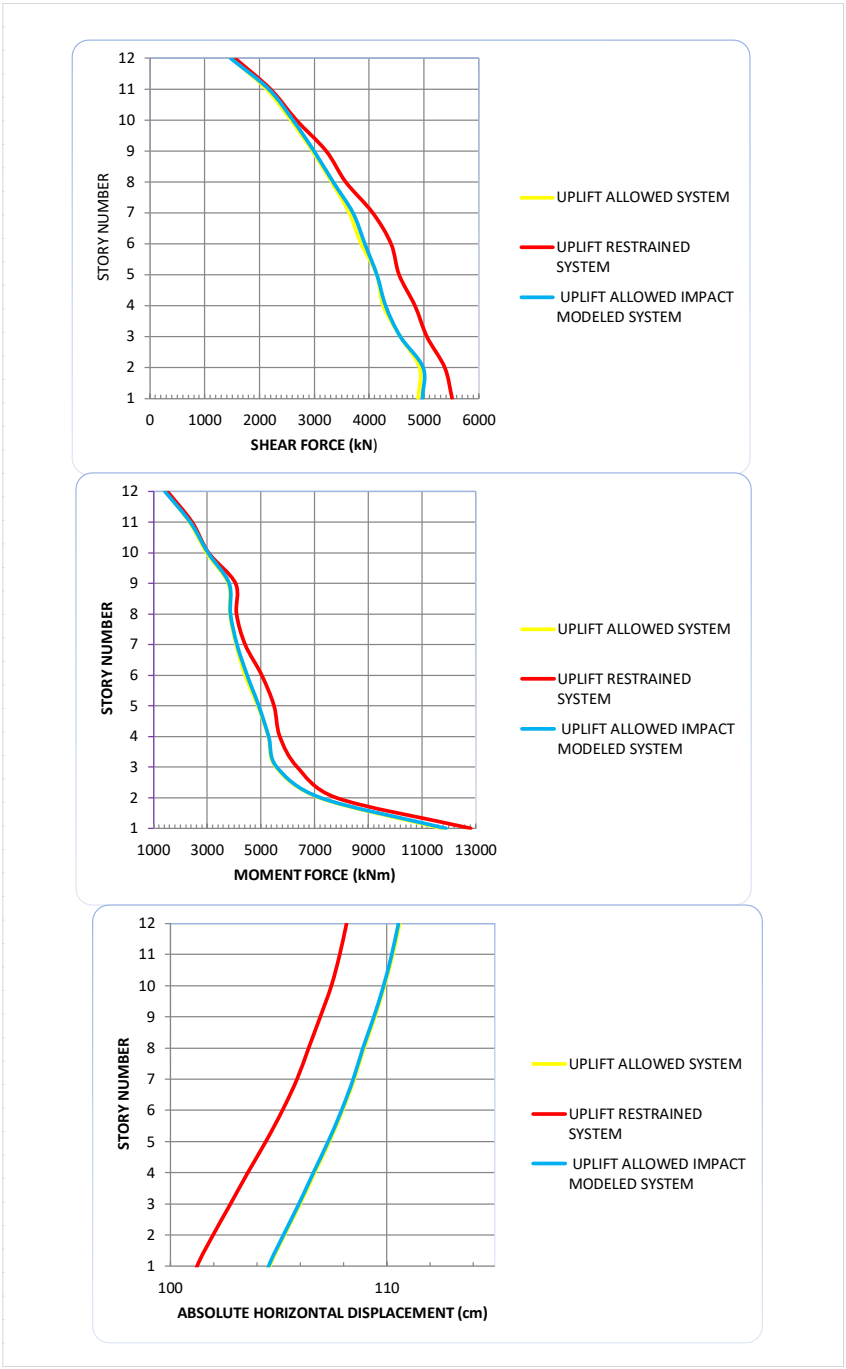

Figure 8.18. Model 21 Analys Results (R=5m, μ= %5, Story Nr=12, Bay Nr=3, PGA=1.6g, Soil Type=C)